Final degree project

Bachelor's degree in Chemical Engineering

NEW STABLE ORGANIC FREE RADICALS WITH AN ELECTRON DONOR-ACCEPTOR MOLECULAR STRUCTURE AS BIPOLAR SEMICONDUCTORS

MEMORY

Author: Gabriel López Calvet
Directors: Lluís Julià Bargés and María Pilar Almajano
Announcement: June 2018

Escola Tècnica Superior
d'Enginyeria Industrial de Barcelona

Abstract

This project deals with the synthesis of two chemical compounds suspected to have good properties for a further application as electronic devices for OLED materials or as a photoelectronic devices for photovoltaic cells (OPV). The synthesis will start from carbazole and tris(2,4,6-trichlorophenil)methyl radical (TTM) for one part, and from 3,6-dibromo-9*H*-carbazole and tris(2,3,5,6-tetrachlorophenyl)methyl radical (DTM) for the other part.

Both radical adducts are formed by a combination of an electron donor-acceptor moieties, resulting on a bigger molecule expected to have interesting magnetic, optical, electrochemical and thermal properties.

Only one radical adduct was successfully synthesized and characterized, showing great results.

Furthermore, the identification techniques applied were Mass spectrometry (ESI-HRMS), Infrared spectrometry (IR) and Nuclear Magnetic Resonance (^{1}H-NMR). Characterization techniques used to analyse radical properties were UV-Visible absorption spectroscopy (UV-Vis), Electron paramagnetic resonance (EPR), Cyclic voltammetry (CV) and Thermogravimetry and Differential Scan Calorimetry (TGA – DSC).

Summary

1. Glossary

μ: magnetic moment

1*:[4-(3,6-diamino-9*H*-carbazolyl)-2,6-dichlorophenyl]bis(2,4,6-trichlorophenyl)methyl radical adduct

2*:[4-(3,6-dibromo-9*H*-carbazolyl)-2,3,5,6-tetrachlorophenyl]bis(2,3,5,6-tetrachlorophenyl)methyl radical adduct

3,6-BrCz: 3,6-dibromo-9*H*-carbazole

3,6-NH_2Cz: 3,6-diamino-9*H*-carbazole

3,6-NO_2Cz: 3,6-dinitro-9*H*-carbazole

A: absorbance

Ar_2: Argon

B_0: external magnetic field

***c*:** concentration

CB: conduction band

Cs_2CO_3: cesium carbonate

CV: cyclic voltammetry

CzTTM: (9*H*-carbazolyl-2,6-dichlorophenyl)bis(2,4,6-trichlorophenyl)methyl radical

DMF: N,N-dimethylformamide

DMSO: dimethyl sulfoxide

DSC: differential scan calorimetry

DTM: tris(2,3,5,6-tetrachlorophenyl)methyl radical

E: potential of an electrochemical cell (V)

E^0: standard potential of an specie (V)

EA: electron affinity

E_{gap}: band gap energy

E_{onset}: onset potential (V)

EPR: electron paramagnetic resonance

EtOAc: Ethyl acetate

eV: electronvolts

g_e: g-factor of the free electron

h: Plank constant

HOMO: highest occupied molecular orbital

I: nuclear spin

IP: ionization potential

LUMO: lowest unoccupied molecular orbital

MOSFET: metal-oxide-semiconductor field-effect transistor

m_s: electron spin

MS: magnetic susceptibility

n: number of electrons

n_a: number of equal magnetic nuclei

OFET: organic field-effect transistor

OLED: organic light emitting diode

OPV: organic photovoltaic cells

OTFT: organic thin layer field-effect transistor

PTM: perchlorotriphenylmethyl radical

T: transmittance

TBAOH: tetrabutylammonium hydroxide

TGA: thermogravimety

TTM: tris(2,4,6-trichlorophenyl)methyl radical

UV-Vis: ultraviolet-visible absorption spectroscopy

VB: valence band

β: Bohr magneton

λ: wavelength

$\boldsymbol{\nu}$**:** frequency (Hz)

2. Introduction

Radicals are a type of molecules where an atom, usually a carbon atom, has an unpaired valence electron. Most of them only exist as transient intermediates occurring during a reaction process. As a result, they are reactive species and many of them spontaneously dimerize (when two identical radical couple together). However, there are some of them that exist as pure liquids or stable solids. This is the case of “stable radicals” or radicals of long life like triphenylmethyl, discovered by Moses Gomberg in 1900, the founder of radical chemistry. [1] This discovery was of great importance because it started the beginning of new studies and investigations on this specific chemistry field that was, in that moment, completely unknown.[2] Triphenylmethyl chemical structure is shown on Fig. 1.

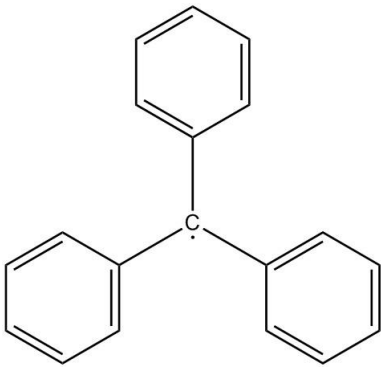

Fig. 1. Triphenylmethyl radical.

The interest of this chemical species is the fact that having an unpaired electron makes the molecule electrically, magnetically and electronically active. This makes some radicals able to perform well as part of products on different fields.

In 1971, Manuel Ballester published the discovery of new stable free radicals, which was awarded with Principe de Asturias award. This discovery was related with perchlorotriphenylmethyl radical (PTM). [3]

Nowadays, there are many persistent radicals already synthesized and characterized. The majority are derived from PTM, tris(2,4,6-trichlorophenyl)methyl radical (TTM) or tris(2,3,5,6-tetrachlorophenyl)methyl radical (DTM), illustrated on Fig. 2. The presence of chlorine atoms in the surroundings of the trivalent carbon atom creates a steric shielding that inhibit both radical-radical reactions and reactions with other reactants.

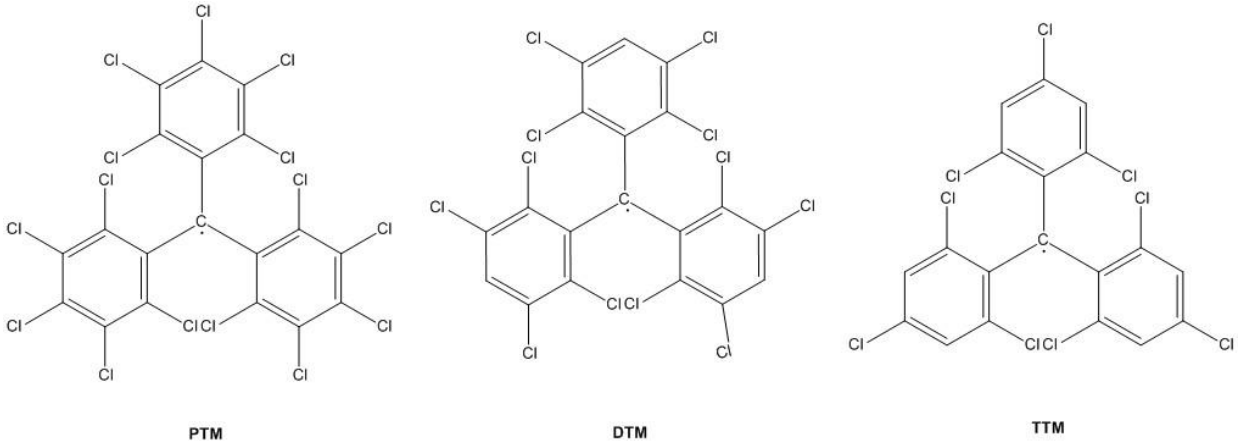

Fig. 2. The most common base for radical series. PTM, DTM and TTM radicals.

The application field for these molecules is very large: they have been used as paint coating for rockets, due to their thermodynamic stability, or for hydrocarbon exploration working as tracers. A more well-known field is electric and electronic area due to their charge-transfer activity, for example solar cells or OLEDs (*organic light-emitting diode*), which will be discussed in more detail on the following pages.

2.1. Motivation behind the project

Despite the fact that this specific research about radicals adducts has already been of great magnitude, there is always the ambition or curiosity to find out new radicals. They can be prepared by modifying ones that are already known and synthesized by adding new functional groups. Inevitably, this is the biggest motivation of this project.

Nevertheless, the possibility of learning about radicals at Institut de Química Avançada de Catalunya (IQAC - CSIC) is a great opportunity for myself to delve into organic chemistry and experimental practice in laboratories due to the highly experimental implication done for elaborate the project.

2.2. Project's scope

This project will show different paths to synthesize [4-(3,6-diamino-9*H*-carbazolyl)-2,6-dichlorophenyl]bis(2,4,6-trichlorophenyl)methyl radical adduct (from now it will be referred as **1**$^{\bullet}$) and it will be characterized using techniques as UV-Vis absorption, Electron Paramagnetic Ressonance (EPR), Cyclic Voltammetry (CV), etc.

In the same way, it will be explained the synthesis and characterization of [4-(3,6-dibromo-9*H*-carbazolyl)-2,3,5,6-tetrachlorophenyl]bis(2,3,5,6-tetrachlorophenyl)methyl radical adduct (from now it will be referred as **2***) (Fig. 3).

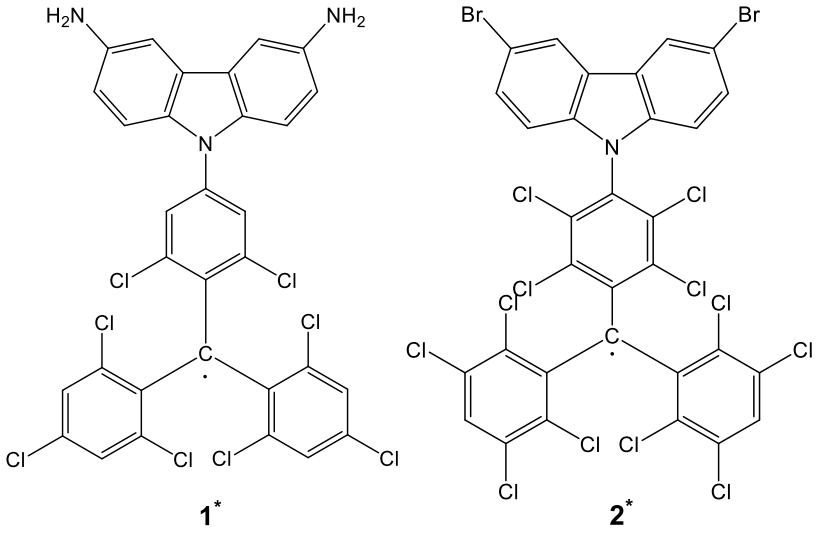

Fig. 3. Structure of radical adduct 1 and 2*.*

In any case, this project will go deeper in how to implement these two new radicals as OLED or any kind of further application, but it will be discussed if the results show good properties to work as semiconductor materials or in electric and electronic applications.

2.3. Objectives

2.3.1. Main objective

The main objective of this project is the synthesis and characterization of two new organic compounds that could be used as semiconductor materials in electronic devices.

These two molecules are radical adduct **1*** and **2***. The first one is formed by electron donor moiety 3,6-diamino-9*H*-carbazole (3,6-NH_2Cz) and electron acceptor moiety TTM. In contrast, the second one is formed by electron donor moiety 3,6-dibromo-9*H*-carbazole (3,6-BrCz) and electron acceptor moiety DTM.

Both of them, which have never been synthesized in the past, are expected to have relevant new physical and electrochemical properties added to those already found in each one of their components.

2.3.2. Specific objectives

The specific objectives are the following ones:

1. A deeply bibliographic review of carbazole, DTM, TTM and its derivatives, for correct comprehension of properties, synthesis and characterization.
2. A bibliographic search of organic semiconductor materials existing nowadays and what makes them relevant in the electronic field.
3. General introduction to chemical reactions involved in this project for a better comprehension of synthesis paths and experimental section.
4. Comprehension of different techniques used for characterise radical adducts (UV-Vis absorption spectroscopy, Electronic Paramagnetic Resonance (EPR), Cyclic Voltammetry (CV) and Thermogravimetry together with Differential Scanning Calorimetry (TGA-DSC).
5. Study the absorption bands of synthesized radicals and discussion of solvent effects.
6. Study magnetic properties of radical adducts with EPR spectra.
7. Study the oxidation and reduction processes from radical adducts with CV.
8. Determine the thermal stability of radical adducts with TGA-DSC.
9. Determine the radical purity of the synthesized compounds with magnetic susceptibility (MS).
10. Give a large economical evaluation of the whole project.
11. Consider the environmental impact of this project through the produced residues, water consumption and CO_2 production.
12. Create a decent project that covers up the diverse aspects involved in the realization of it.

3. Theoretical basis

3.1. Theory of used chemical reactions

As it will be read on the experimental section, the chemical reactions done in this project consist in five different types. These will be introduced just below:

3.1.1. Radicalization reaction

As all the stable radicals used in this project are photosensitive compounds when they are in solution, the radicalization needs to be done in dark. In the same way, something similar happens with atmosphere, as the oxidized form of these radicals are stable too. Consequently, this type of reaction needs to be done under an inert atmosphere like Ar_2 or N_2.

Otherwise, this reaction is done in two steps, the first one with tetrabutylammonium hydroxide 1.5 M (TBAOH), an organic base that compared to more conventional inorganic bases, such as KOH and NaOH, is more soluble in organic solvents. The second step is done with chloranil, an electron acceptor, which finally gives the expected radical. The dissolvent used is tetrahydrofuran (THF).

This procedure has been followed for a while in different projects and investigations resulting on a successful path to synthetize radicals. [4]

3.1.2. Coupling reaction

Coupling reactions need the organic compound in the radical form, so it is necessary to take the same precautions written in the above section, such as inert atmosphere and low luminosity. Furthermore, anhydrous cesium carbonate (Cs_2CO_3), used as base in organic synthesis, and N,N-dimethylformamide (DMF), which dissolve all the solids, are mixed with reactants.

3.1.3. Nitration reaction

Nitration reactions can be done with different methodologies, for example, using a mixture of nitric acid (HNO_3) with sulfuric acid (H_2SO_4) or HNO_3 with acetic acid (AcOH). In this project, 1,2-dichloroethane is used as dissolvent and only fuming HNO_3 is used as nitration agent. This methodology was chosen because it has been proven that for carbazole nitration, good yields were achieved (85 - 98 %). [5]

3.1.4. Reduction reaction

There are two different methods to obtain an amino group from nitro compounds: one is a hydrogenation reaction with H_2 gas and Ni/Pt, and the other one is a reduction reaction with an acid and a metal. The conditions of the second reaction are more optimal, for this reason this will be the chosen methodology. In addition, hydrogenation reduce C=C bounds, so it could react with the benzene moiety.

As it will be seen on the experimental section, $SnCl_2$ is used as metal. For the acid solution, it can be used a mixture of AcOH or EtOH with HCl.[6]

Another type of reaction that will be written in this project is the conversion of radical to hydrogenated compound (αH compound). This was done with ascorbic acid, the protonation reagent, and a solution of THF with distilled water. [7]

3.2. Carbazole

Carbazole (Fig. 4) is an aromatic heterocyclic organic compound, which has a nitrogen atom in one of its cycles. More concretely, it has a tricyclic structure, two benzene rings fused on either side of pyrrolidine. In the ultraviolet spectrum, the low-lying n → π* transitions in the electronic spectrum involving the nonbonding electrons on nitrogen have properties similar to those of π → π* transitions. This is why carbazole is a fundamental chromophore that gives an efficient emission at λ ~ 340 nm in dilute solutions, corresponding to the monomeric molecule.

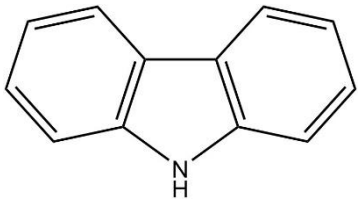

Fig. 4. Carbazole.

The synthesis and applications of carbazole derivatives have been a source of great interest for chemists and materials scientists due to their intrinsic photophysical and redox properties. They exhibit relatively intense luminescence and high photoconductivities and also undergo reversible oxidation processes making them suitable as hole carriers. Consequently, carbazoles are widely used as building blocks for potential organic semiconductors. Hence, the addition of carbazole moieties into a polymeric chain can significantly improve photoconductivity and hole carrying properties. For example, in the field of OLEDs, carbazoles are used as materials for hole-transporting and light-emitting layers. [8]

Furthermore, carbazole ring can easily be functionalized and covalently linked with different substituents (as halogen atoms, nitro groups, etc.) on aromatic positions from benzene. However, the poor nucleophilic assistance of nitrogen's unpaired electrons makes any incorporation into aromatic systems challenging. Thus, it is necessary to tighten the reaction conditions to succeed with it. [9]

3.3. Radical adducts

Radical adducts are a special type of organic molecules due to their specific properties because they combine particular characteristics of each molecule which is composed of. In fact, they are formed by electron donor-acceptor moieties, which classifies them as organic charge-transfer compounds. Concretely, this property has made radical adducts of great interest and they have been studied for a while. This is the case of Nutraceuticals and Free Radicals (NFR) investigation group, which has been publishing and studying the electrochemical and photoluminescent properties of this new family of radical adducts, where the donor part was formed by carbazole or its derivatives, and the acceptor part was TTM, DTM or PTM.

For example, [4-(9*H*-carbazolyl)-2,6-dichlorophenyl]bis(2,4,6-trichlorophenyl)methyl radical (referred as CzTTM along the project), which will be an intermediate in the unsuccessfully synthesis of **1***, has shown attractive electrochemical properties with quasi-reversible processes either in the anodic or in the cathodic region to give cationic or anionic species, respectively, with excellent stability. [9]

As an element belonging to the series of TTM radical, it is expected that the stability of **1*** is due to the steric hindrance of six chlorine atoms around the trivalent carbon. All of these radicals are completely disassociated (they do not dimerize) and present a large stability either in solid or in solution, despite the fact that in solution, they are photosensible. Hence, they do not abstract H-atoms from hydrogen-labile species, but they are very sensitive to electron-transfer reactions, being easily reduced to anions and oxidized to cations in the presence of electron-donor and acceptor species, respectively. Therefore, the stability of the charged species is comparable to that of their radical precursors. [4]

The same is expected in the case of DTM series, or more specifically, radical adduct **2***, which was synthesized and characterized successfully. The main difference between DTM and TTM radicals is that DTM has chlorine substituents in *orto* and *meta* positions.

Radical adduct **2*** is formed by DTM as the electron-acceptor open-shell moiety, and a

heterocycle such as 3,6-BrCz, as the electron-donor moiety. The new radical adduct has significant physical and electrochemical properties, as well as its intrinsic magnetic character due to molecule's trivalent carbon. Furthermore, the combination of 3,6-BrCz with DTM has been revealed as an efficient strategy to obtain ambipolar transport properties, the ability to transport either positive charges (holes) and negative charges (electrons).

3.4. Intramolecular charge-transfer

As it was said on chapter 3.3, pure organic charge-transfer molecules are composed mainly of electron donor-acceptor moieties.

In the charge-transfer excited state, the electron moves from the donor to the acceptor part of the molecule, and this resulting electrostatic attraction created by an excess of positive and negative charge in different parts of the molecule, provides a stabilizing force for the molecular.

The two redox centres of the molecule, the donor and the acceptor, may be directly bonded or linked through a saturated or unsaturated bridge connecting both centres, and the energy of the excitation, the energy difference between the exited and the ground state, strongly depends on the nature and length of the bridge between them. If the excitation energy decreases, charge-transfer band is bathochromically shifted towards the visible and near infrared part of spectrum. Furthermore, organic charge-transfer compounds play a significant role in the chemistry of materials and have found use as sensitizers for dye-sensitized solar cells. [10]

3.5. Radical adduct implementations

According to what it has been slightly mentioned heretofore, radical adducts have relevant implementations on electric – electronic field as semiconductor materials working on devices as *organic light-emitting diode* (OLED), *organic photovoltaic cells* (OPV) or *organic field-effect transistor* (OFET). Before entering in more detail about each implementation, an introduction to semiconductor materials will be done.

3.5.1. Semiconductor materials

Semiconductor materials are one of the three different types of materials existing depending on electrical properties. They can be classified as conductors, semiconductors or insulators according to the availability of conduction electrons in their structures. Band theory gives an explanation for these differences in electrical properties and accounts for the availability, or not, of those conduction electrons.

There are such enormous numbers of electrons in a solid mass that although the bands actually consist of very large numbers of closely packed discrete energy levels, the bands become essentially continuous. There may be several permitted energy level bands, but in particular we consider the two uppermost bands. These are known as the valence band (VB) and the conduction band (CB) (Fig. 5).

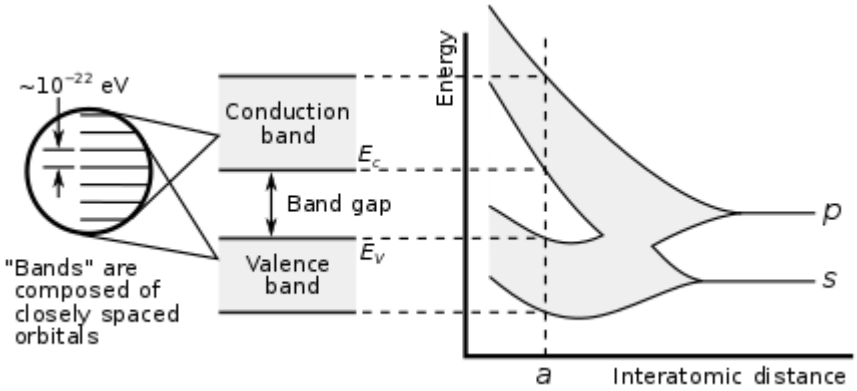

Fig. 5. On the left part, there is a representation of VB and CV. On the right part, it is shown energy levels as function of the spacing between atoms. [11]

VB is filled with outer shell atom electrons and CB is formed by free electrons that can move easily through the solid. These electrons are responsible of leading electricity. Between this two band there is a band gap (BG), also called forbidden gap, because is impossible to find any electron on it. [12], [11]

In insulators, the electrons in the valence band are separated by a large gap from the conduction band (greater than 2 eV). In conductors, like metals, the valence band overlaps the conduction band, and in semiconductors there is a small enough gap between the valence and conduction bands that thermal or other excitations can bridge the gap (between 1 and 2 eV).

When an electron jumps to CB, it generates, at the same time, a hole in the VB. Holes act as charge carriers too because when an electron takes its place, the hole moves to the positon

where the electron came from. This phenomenon, where an electron moves from VB to CB (called ionization), only happens when an electron absorbs a higher energy than band gap energy (E_{gap}).

Finally, traditional semiconductors are rarely used as pure materials (intrinsic semiconductors) and they are doped with impurities to diminish E_{gap} energy (extrinsic semiconductors). If these impurities are electron-donor atoms, it is called n-type. Conversely, if these impurities are electron-acceptor atoms, it is called p-type. In both cases conductivity is increased, one with extra electrons and the other one with extra holes, respectively. [13]

In the case of organic semiconductors, it is crucial they have π conjugated systems (for electron delocalization), low E_{gap} values, stability, purity and solubility in organic solvents.

3.5.2. Organic light-emitting diode (OLED)

Organic light-emitting diodes (OLEDs) are based on electroluminescence phenomenon, which is light emission from a material due to current flow through it. Thus, this material has to drive current and emit light when electron returns from his exited to his normal state. The last property is due to radiative electron - hole recombination in the organic layer (charge carriers are eliminated emitting energy).

The simplest OLED consists of a thin layer of organic material sandwiched between two metal contacts. The organic layer is not doped and the asymmetry of the contacts determines the diode nature of the device. [14]

These devices are of interest for displays because they show promise for low cost, large area devices, and they are compatible with low processing temperatures and flexible substrates.[15]

3.5.3. Organic photovoltaic cells (OPV)

Organic photovoltaic cells (OPV) have an analogous structure to OLED in spite of doing the opposite function, which is converting photons to electricity due to photovoltaic effect.

Organic material thin layer consist of a nanostructured blend of donor (n-type) and acceptor (p-type) semiconductors (Fig. 6), creating the bulk heterojunction (comparable to p-n junction in inorganic semiconductors). [16] When either semiconductor absorbs photons, molecular excitons emerge. Excitons are an electrically neutral quasiparticle formed by an electron and a hole, which are attracted to each other by the electrostatic Coulomb force.

These excitons are an important intermediate in the solar energy conversion process because when they dissociate, free charge carriers are created. These ones are the desired final products for photovoltaic conversion, as they generate the expected electrical field when they

travel to their respective electrode. [17]

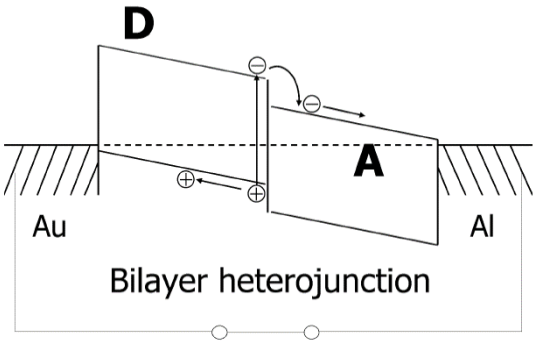

Fig. 6. Schematic of a bilayer heterojunction device. [18]

OPVs can be added to any plastic surface as an ultrathin layer. In addition, they are cheaper and lighter than conventional ones. Nevertheless, efficiency and electric resistivity are not tremendous, which is still keeping OPVs behind inorganic ones.

3.5.4. Organic field-effect transistors (OFET)

Organic field-effect transistors (OFETs) are analogous to well-known MOSFET, differing only on channel material used, as it is implemented with an organic semiconductor instead of an inorganic one. There are diverse types of OFETs structures and consequently, it will be explained *organic thin film transistors* (OTFTs).

OTFT is a three-terminal device, in which a voltage applied to a gate electrode controls current flow between a source and drain electrode under an imposed bias. A basic schematic is shown in Fig. 7, where V_g and V_{ds} are the applied gate and source-drain voltages, respectively. The control of source-drain current in FETs via a third terminal has resulted in their widespread use as switches. [19]

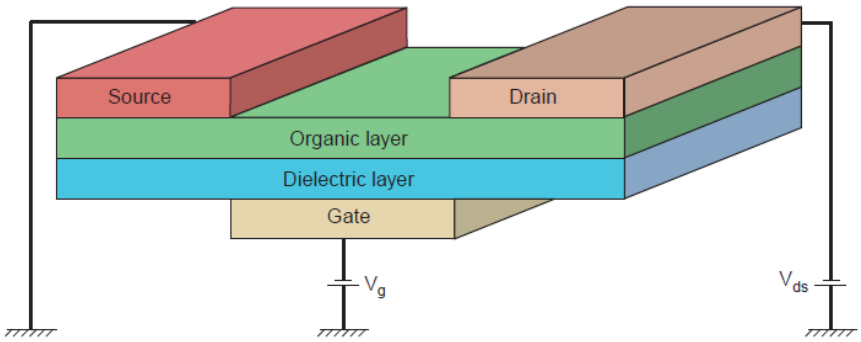

Fig. 7. Basic schematic of a field-effect transistor. [19]

Organic transistors are potentially useful for applications that require electronic functionality with low or medium complexity distributed over large areas on unconventional substrates, such as glass or flexible plastic film. Generally, these are applications in which the use of single-crystal silicon devices and circuits is technically or economically not feasible. In other cases, the use of silicon MOSFETs is very economical and more reasonable than organic ones. [20]

3.6. Synthesis of radical adduct 1*

To synthesize radical adduct **1*** it was tried three different synthetic paths. Despite not being possible to obtain the final product **1***, the different synthesis tried will be described in the following section.

3.6.1. Synthesis path 1

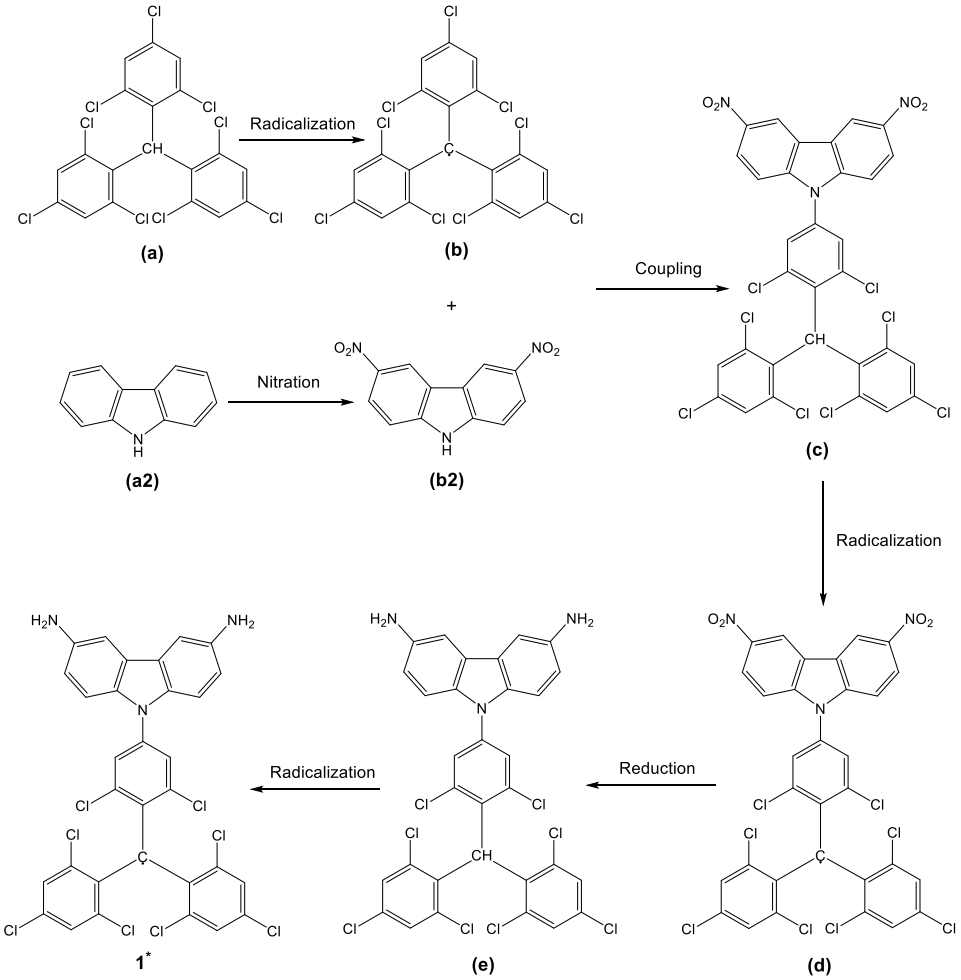

Fig. 8. Synthesis path 1 description.

Fig. 8 describes the first synthesis path followed. It starts converting αHTTM *(a)*, already

synthetized by NFR research group, to its radical form TTM *(b)*, and at the same time, carbazole *(a2)*, which is a commercial product, to 3,6-NO_2Cz *(b2)*. On one hand, as it was explained on chapter 3.1.1, for the radicalization reaction TBAOH is added to extract α-hydrogen from the central carbon to give TTM anion form, and with the further addition of chloranil, TTM anion is transformed to TTM radical. On the other hand, as it was explained on chapter 3.1.3, for the nitration reaction fuming HNO_3 is added as nitration agent, which attacks 1, 3 and 6 positions of *a2*, giving two different isomers, despite only being 3,6-NO_2Cz interesting.

Next step is the coupling reaction between *b* and *b2,* as it was introduced on chapter 3.1.2. At this point, the first problem appeared because this reaction was unsuccessful. It is thought that nitro groups, as they are electron acceptor groups, makes 3,6-NO_2Cz anion, which is a reaction intermediate, stable and less reactive, making the reaction complicated to succeed.

If it had been possible to continue though this point, a radicalization of αHNO_2CzTTM *(c)* would have been the next step, followed by a reduction reaction to obtain αHNH_2CzTTM *(e)*.

Finally, the last part would have been converting *e* to **1**$^{\bullet}$ with another radicalization reaction.

3.6.2. Synthesis path 2

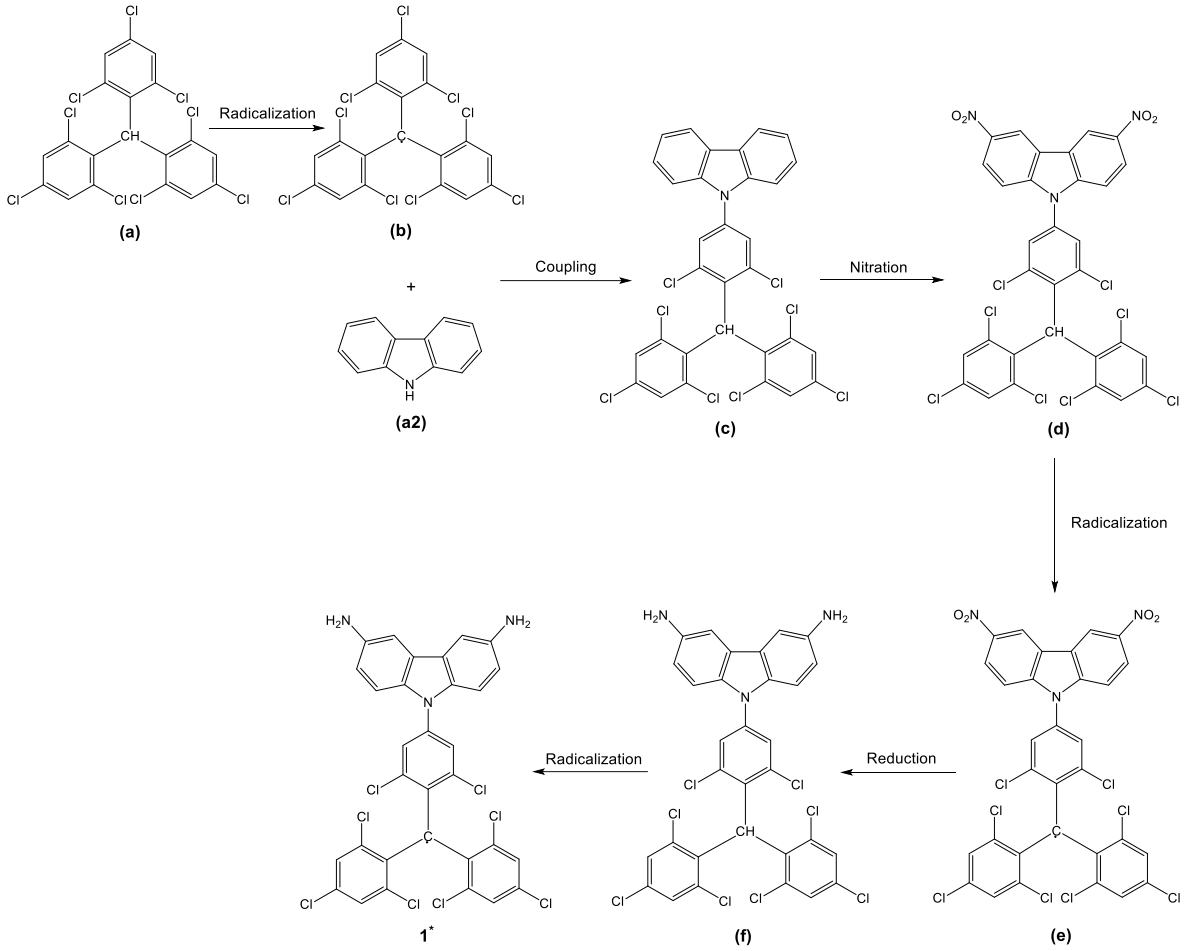

Fig. 9. Synthesis path 2 description.

Fig. 9 describes the second synthesis path followed. It also starts converting αHTTM *(a)* to TTM radical *(b)*, as it was explained on the last section, but this time carbazole *(a2)* is directly coupled with *b* to give αHCzTTM *(c)*. Then, before starting the nitration reaction, the coupling product was reduced with ascorbic acid, as it was explained on the last part of chapter 3.1.4. This was done to guarantee a better yield at the nitration reaction. Once αHNO_2CzTTM *(d)* was synthetized (this time 1,6-dinitro-9*H*-carbazole isomer (1,6-NO_2Cz) did not appear because of steric difficulties, but mononitration product was formed) a radicalization reaction was done to obtain NO_2CzTTM radical *(e)*.

The next problem started at this point, when reduction of *e* was tried twice with different synthesis methodologies and none of them worked.

Finally, it would have been a last radicalization reaction because previous reduction would have affected trivalent carbon radical too. After being unable to solve this problem, a third synthesis path was tried.

3.6.3. Synthesis path 3

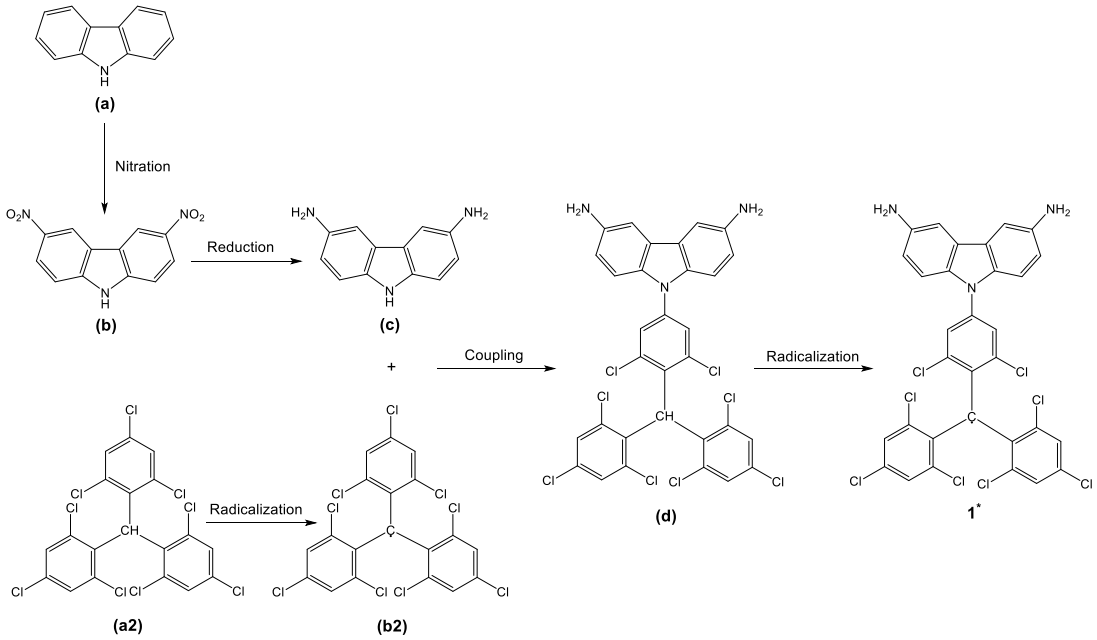

Fig. 10. Synthesis path 3 description.

Fig. 10 describes the third and the last path tried to synthesize **1***. The novelty, which diverge from the first synthesis path, is reduction of b to 3,6-NH_2Cz *(c)*, which was explained on first part of chapter 3.1.4. $SnCl_2$ was used as a reducing agent and solvent mixture, AcOH and HCl, was also acting as protonation agent. This gave the 3,6-NH_2Cz dichlohydrate intermediate, which was soluble in acid medium, and with a further neutralization c was synthesized.

The problem started again with coupling reaction. As it did not take place, it was not possible to synthesize (*d)* and in addition, neither **1***.

3.7. Synthesis of radical adduct 2*

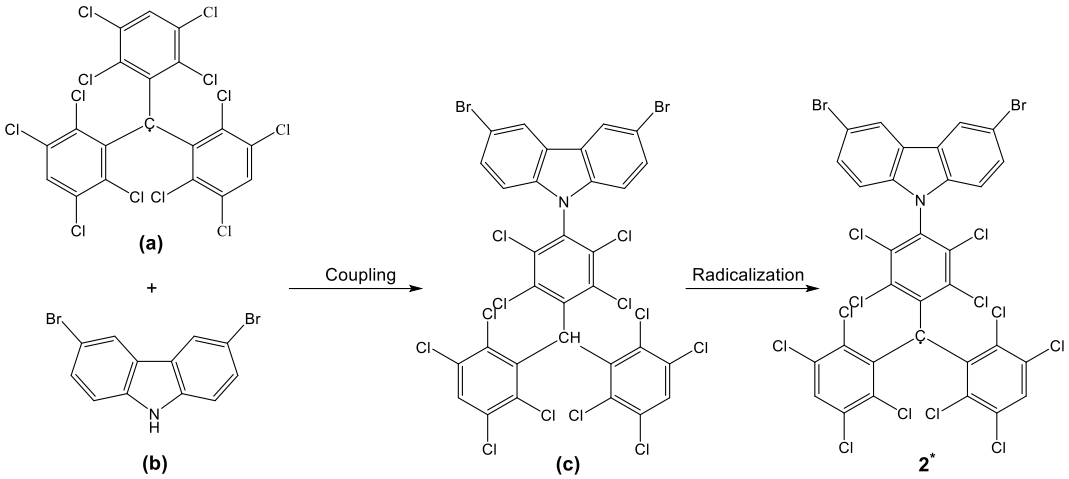

Fig. 11. Synthesis path for radical adduct 2.*

Fig. 11 represents synthesis path of radical adduct **2***. It starts with a coupling reaction of DTM radical *(a)*, already synthesized by NFR research group, and 3,6-BrCz *(b)*, a commercial product. This gives αHBrCzDTM *(c)* that with a further radicalization becomes **2***. This synthesis did not bring any problem, as everything worked well on the first try.

3.8. Characterization techniques

3.8.1. Study of optical properties with UV-Vis absorption spectroscopy

In this chapter is explained UV-Visible spectroscopy theory because this technique will be used for characterize radical adduct **2***.

This technique is associated with excitation of electrons from lower (ground state, occupied molecular orbital) to higher (exited state, unoccupied molecular orbital) energy levels. With the help of electromagnetic radiation (light beam) is given the precise amount of energy to cause these transitions, as the molecule will only absorb light if the energy of the photons of light matches the difference in energy between the two orbitals involved in the transition.

Therefore, as visible and ultraviolet region are between 200–800 nm (λ), only nonbonding outer electrons (n) from atoms as O, N or halogens, and π orbital electrons will suffer energetic transitions to an antibonding π orbital (π*) (n → π* and π → π* transitions respectively). This is represented on Fig. 12.

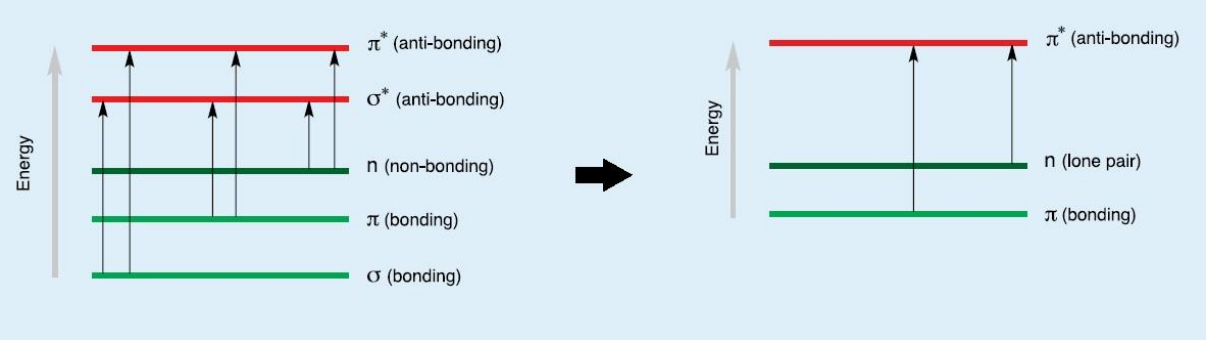

Fig. 12. On the left part is represented different electron transition that a molecule can have. On the right part is represented only the transitions affecting UV-Vis range.

In addition, compounds that have a high degree of conjugation (a series of overlapping p-orbitals that result in the delocalization of charge, usually in alternating single and multiple bonds) will absorb at longer wavelengths and as such are often coloured. [21] This is the case of TTM and DTM radical series.

These transitions are drawn in UV-Vis spectrum, where absorbance (A, dimensionless) is represented against wavelength (λ, nm). These spectres can be affected by five different factors:

- High sample concentrations: molecular interactions (for example, polymerisation) can take place causing changes to the position and shape of absorption bands. Such an outcome can affect the linearity of the relationship between sample concentration and absorbance, as will be seen further with Lambert-Beer law.

- pH variations: the pH of the sample solution can have a significant impact on absorption spectrum. The mechanism for this is primarily a shift in the equilibrium between the different chemical forms of an analyte.

- Photochemical reactions: when an analyte is photosensible, it is necessary to consider this fact and protect it from the light. Concretely, this is the case of radical adducts.

- Temperature: this can affect in different ways absorption measurements like expansion or contraction of the solvent (leading to lower/higher absorbance) or shifts in equilibria between the chemical forms of an analyte (thermochromism).

- Solvent effect: the choice of solvent can shift peaks to shorter or longer wavelengths. This will depend on the nature of the interaction of the particular solvent with the environment of the chromophore (chemical functional groups capable of exhibiting

characteristic absorptions in the UV and visible regions of the spectrum) in the excited state of the molecule. Depending on the chromophore in the particular analyte, changes in the polarity of the solvent can influence shifts to longer or shorter wavelengths.

For a specific wavelength, absorbance (A), transmittance (T) and concentration (c) are related together with Lambert-beer law.

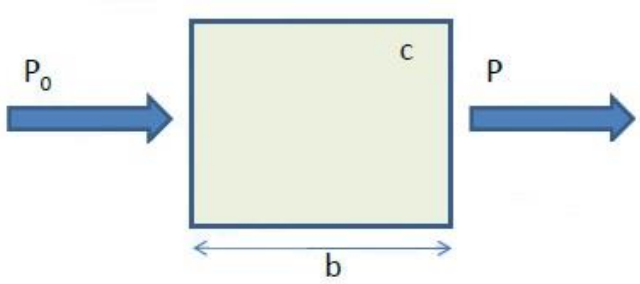

Fig. 13. Schematic of sample analysis. The incident radiation (P_0) passes through a cuvette, which absorbs part of it.

The transmittance (T) of the solution is the fraction of incident radiation transmitted by the solution and is often expressed as a percentage, the absorbance (A) is defined as minus logarithm of T and Lambert-beer equation relates lineally A with concentration (c). All this is written together in Eq. 1.

$$A = -logT = log\frac{P_0}{P} = \varepsilon bc \quad \textit{(Eq. 1)}$$

P_0 is the original power of the beam and P is the remaining power after passing through the sample; b (cm) is the optical path length of radiation, or also the cell length where the solution is kept; and ε ($L \cdot mol^{-1} \cdot cm^{-1}$) is called the molar absorptivity, which is independent of sample concentration. Fig. 13 represents a simple scheme of the phenomena.

With this equation is possible to determinate an unknown sample concentration with a previous calibration with pattern samples. [22]

Finally, the UV-Vis spectrometer is formed by four parts: a light emitting source (a combination of tungsten/halogen and deuterium lamps), a monochromator (which splits the initial beam into its component wavelengths), a cuvette where the sample is introduced, and the detector, which transforms the optical signal into an electrical one. [23]

3.8.2. Study of magnetic properties with EPR

Determination of magnetic properties from the organic radicals has been done with Electron Paramagnetic Resonance (EPR).

This spectroscopy technique is concerned with the study of species containing one or more unpaired electrons and hence it can be applied to the study of radicals. The principles underlying EPR are very similar to those of NMR spectroscopy: a molecule or atom has discrete states, each of them with a corresponding energy, and the measurement and interpretation of the energy differences between the atomic or molecular states is called spectroscopy.

It is possible to measure these energy differences, ΔE, because of an important relationship between ΔE and the absorption of electromagnetic radiation. According to Planck's law (Eq. 2), electromagnetic radiation will be absorbed if:

$$\Delta E = h\nu \quad \textit{(Eq.2)}$$

Where *h* is Planck's constant and ν is the frequency of the radiation.

In EPR, electron spins are excited instead of spins of atomic nuclei as it is in NMR. The interaction of an external magnetic field (B_0) with an electron spin (Zeeman effect) depends upon the magnetic moment associated with the spin (μ). The only two possibilities for electron spin orientation are -½ and ½, m_s values for parallel and antiparallel respectively. [24]

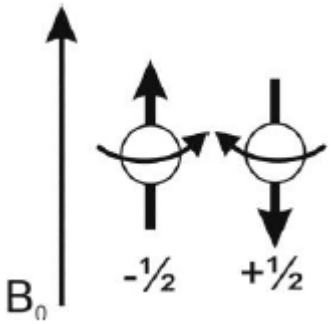

Fig. 14. Minimum and maximum energy orientation of μ with respect to the magnetic field, B_0. [25]

When the electron moment is aligned with the magnetic field, its energy state is lower than it is aligned against the magnetic field, as it is shown on Fig. 14.

As a result, there are two energy states (Eq. 3, Eq. 4, Eq. 5):

$$\Delta E = \mu B_0 = m_s g_e \beta B_0 \quad \textit{(Eq. 3)}$$

$$\Delta E_{1/2} = \tfrac{1}{2} g_e \beta B_0 \quad \text{and} \quad \Delta E_{-1/2} = -\tfrac{1}{2} g_e \beta B_0 \quad \textit{(Eq. 4, Eq. 5)}$$

Where g_e is a dimensionless proportionality constant, often referred as g-factor of the free electron (≈ 2.0023), and β is the Bohr magneton ($= eh/4\pi m_e$, where e and m_e are the charge

and mass of the electron respectively). This is illustrated on Fig. 15:

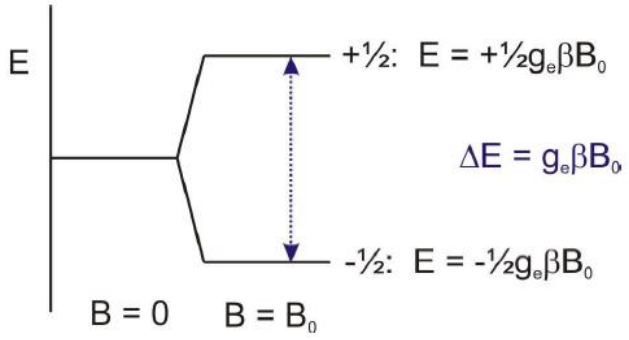

Fig. 15. Introduction of the spin state energies as a function of the magnetic field B_0. [25]

However, the magnetic moment μ, when the electron is not free and is into a molecule, changes caused by a phenomenon called spin–orbital interaction. This depends on the spin-orbit coupling contribution, that it is affected by the size of the nucleus containing the unpaired electron. Therefore, organic free radicals, with only H, O, C and N atoms, would have a small contribution from spin-orbit coupling, producing g-factors very close to g_e while the g-factors of much larger elements, such as metals, may be significantly different from g-factor of the free electron. In conclusion, every radical has a specific g-factor in function of its structure. [26]

In practice, for the study of organic radicals, the frequency is a fixed one (inside the microwaves range) and the external magnetic field is modified. When resonance happens is because emitted radiation energy matches the energy between the two electron spin states and the electron absorbs it ($\Delta E = g\,\beta B_0$).

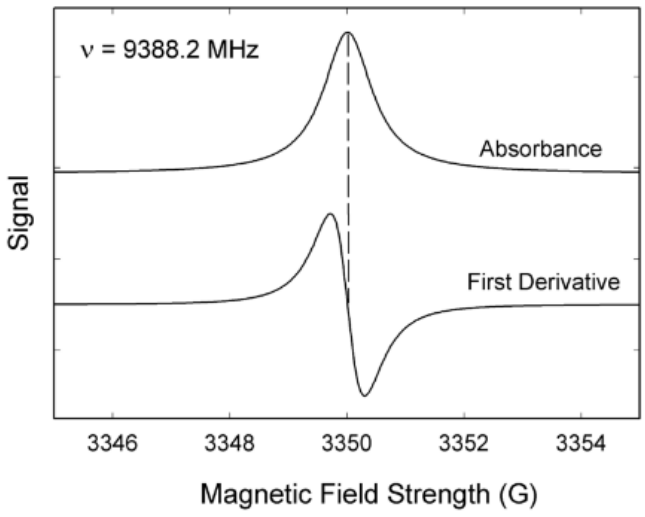

Fig. 16. Example of EPR spectrum. On the top, absorption curve. On the bottom, first derivate of absorption curve. [27]

As a result, it is possible to detect this absorption and EPR are arranged to record the first derivate of the absorption curve, as it is exhibited above Fig. 16, rather than the absorption curve itself. This gives somewhat greater sensitivity and better resolution.

EPR spectra are characterized by three parameters:

- **g-factor**: In addition of all said before about this constant, it is important to know that g-factor is an anisotropic value (direction dependent, it is a vector). This is important when the sample analysed is a crystal: it would be found out that g-factor of the EPR spectrum would change as it is rotated in the spectrometer. Nevertheless, as radicals discussed in this project are stable in solution, this property from g-factor is negligible due to all of this anisotropy is averaged out. As a result, it is a scalar value.

- **Hyperfine splitting**: Hyperfine splitting results of magnetic coupling between unpaired electron spin and those nearby magnetics nuclei that contains the molecule ($I \neq 0$). The number of level transitions resulting from coupling with n_a equal magnetic nuclei is $2In_a + 1$. For example, methyl radical has tree equivalent magnetic hydrogens. Thus, EPR spectrum is a 1 : 3 : 3 : 1 quartet (^{1}H, $I = \frac{1}{2}$) as it is illustrated on Fig. 17.

  The separation of two lines is known as the hyperfine coupling constant or hyperfine splitting constant: it is measured in millitesla (mT) using SI, or in gauss (G)
  (1 mT = 10 G).

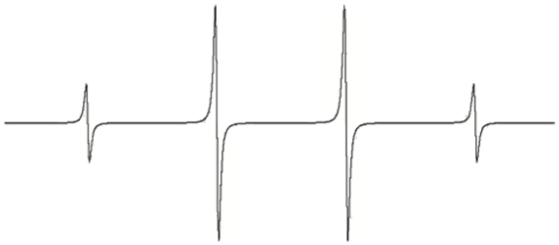

Fig. 17. Theoretical CH_3 radical EPR spectrum. [28]

- **Line width (ΔH_{pp})**: Line width is the difference between the maximum and the minimum from first derivate, also measured in militeslas (mT). It is related with spin behaviour after energy absorption and it is function of register temperature and sample concentration. Concretely, it is directly proportional to temperature, because when temperature decreases, a better peak resolution is achieved, as the line width is also reduced.

3.8.3. Study of redox properties with cyclic voltammetry (CV)

Redox properties from radical adducts are studied by an electrochemical method called cyclic voltammetry.

Cyclic voltammetry (CV) is a powerful and popular electrochemical technique commonly employed to investigate the reduction and oxidation processes of molecular species.

The trace A in Fig. 18 is called voltammogram or cyclic voltammogram, in this case the ferrocene one. The x-axis represents a parameter that is imposed on the system, the applied potential (E), while the y-axis is the response, the resulting current (I) passed. The arrow indicates the beginning and sweep direction of the first segment (or "forward scan"). Another important parameter in a voltammogram is the scan rate, which indicates the speed of potential variation (linearly) during the experiment (expressed in mV/s). Trace B represents the relationship between time and applied potential.

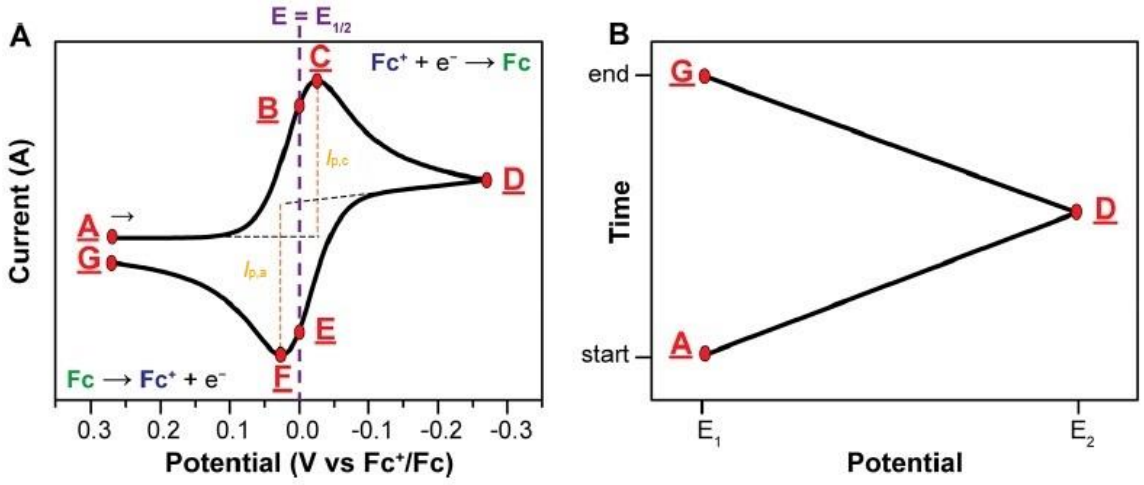

Fig. 18. At the left, Ferrocene voltammogram. At the right, a graph of potential evolution in function of time. [29]

In this example, in the forward scan, the potential is swept negatively from the starting potential E_1 to the switching potential E_2. This is referred to as the cathodic trace, which is a reduction reaction. The scan direction is then reversed, and the potential is swept positively back to E_1, referred to as the anodic trace which is an oxidation reaction of the product formed by the previous reduction.

This specific profile in voltammograms is due to Nernst equation, which relates the potential of an electrochemical cell (E) to the standard potential of a species (E^0) and the relative activities of the oxidized (Ox) and reduced (Red) analyte in the system at equilibrium. In Eq. 6, *F* is Faraday's constant, *R* is the universal gas constant, *n* is the number of electrons, and *T* is the temperature.

$$E = E^0 + \frac{RT}{nF} ln \frac{[Ox]}{[Red]} = E^0 + 2.3026 \frac{RT}{nF} log \frac{[Ox]}{[Red]} \quad (Eq.\ 6)$$

The maximum and the minimum values of potential (cathodic peak and anodic peak, $E_{p,c}$ and $E_{p,a}$, marked as C and F on Fig. 18, respectively) are two important values from the oxidation and reduction process. If it is assumed the process is chemically and electrochemically reversible, it can be calculated the number of transferred electrons, as it is written in Eq. 7.

$$E_{p,a} - E_{p,c} = \frac{2.22RT}{nF} = \frac{59}{n} \quad (Eq.\ 7)$$

On one hand, chemical reversibility is used to denote whether the analyte is stable upon reduction and can subsequently be reoxidized. On the other hand, electrochemical reversibility refers to the electron transfer kinetics between the electrode and the analyte. When there is a low barrier to electron transfer is electrochemically reversible. Repeating the analysis at different scan rates and checking for each repetition that the $I_{p,c}$ and $I_{p,a}$ (marked on Fig. 18) are of the same magnitude order, ensures this type of reversibility. [30]

In addition, it is possible to calculate electron affinity (EA) and ionization potential (IP) with Eq. 8:

$$IP, EA = E_{\text{onset vs Ag/Ag}^+} + 4.6 \quad (Eq.\ 8)$$

As it was used an Ag/Ag+ reference electrode, 4.6 eV is the energy difference between vacuum and this RE, and E_{onset} is the value where the reduction/oxidation reaction starts (calculated graphically).

With IP and EA, using Eq. 9, it can be obtained the electrochemical band gap (E_{gap}) that is the difference between HOMO and LUMO orbitals:

$$E_{gap} = IP - EA \quad (Eq.\ 9)$$

Furthermore, instrumentation for CV analysis is composed of an electrochemical cell (with three different electrodes and an electrolyte solution, as can be seen on Fig. 19), a potentiostat, a voltage to current converter and a data acquisition system.

The three different electrodes are: the working electrode (WE), which carries out the electrochemical event of interest and it is composed of redox inert material in the potential range of interest; the reference electrode (RE) has a well-defined and stable equilibrium potential. It is used, as its name says, like a reference point against which the potential of other electrodes can be measured in an electrochemical cell; the counter electrode (CE), which completes the electrical circuit between WE and CE. [29]

Finally, the electrolyte solution is formed by the analyte, the solvent and an extra salt called supporting electrolyte that increase solution conductivity.

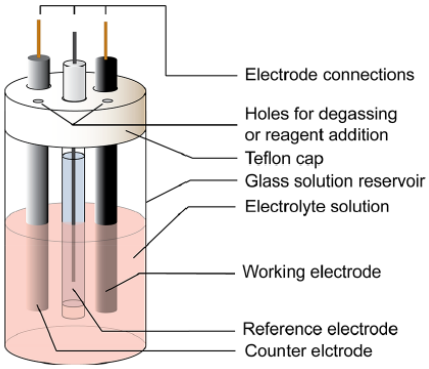

Fig. 19. Cyclic voltammetry analysis cell. [29]

3.8.4. Study of thermal properties with TGA and DSC

Thermal properties of radical adduct **2*** will be studied with differential scanning calorimetry (DSC) and thermogravimetric analysis (TGA).

On one hand, DSC measures various thermal transitions associated with a material when it is heated or cooled in a controlled manner. The thermal transition could be due to a physical transformation or a chemical reaction. Physical transformations, such as melting, crystallization, polymorph conversion, desolvation, and dehydration, are always associated with a change in enthalpy. This change of enthalpy is detected as a heat-absorbed (endothermic) or heat-released (exothermic) event in DSC. The thermal events associated with melting, dehydration, or desolvation are directly related to the crystal structure of a material, and therefore, provide fundamental information related to its crystal structure. [31]

The graphic obtained by DSC is called thermogram and is plotted as heat flow versus temperature. On Fig. 20 is shown DSC scan of PET.

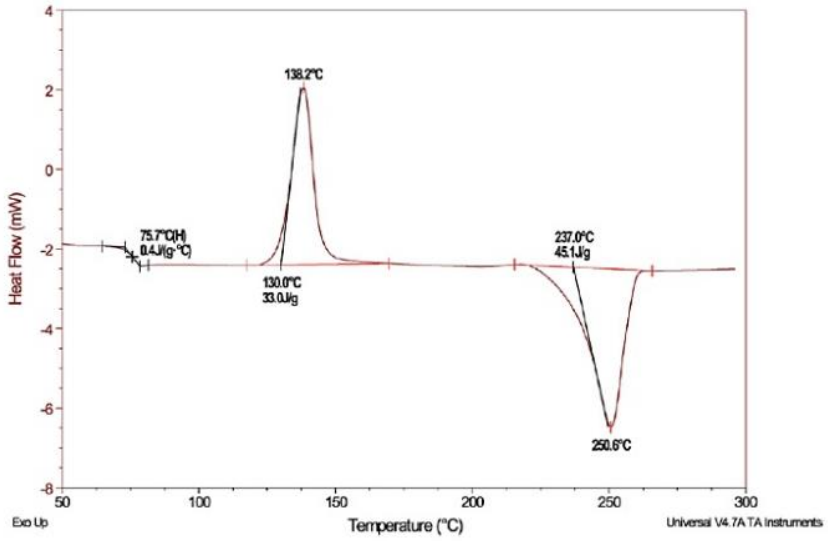

Fig. 20. Thermogram of PET DSC scan. [32]

On the other hand, TGA is used to measure mass changes of a material as a function of time at a selected temperature (i.e., isothermal mode), or over a particular temperature range using a predetermined heating rate under a controlled atmosphere, as it will be the case of radical adduct analysis. TGA is carried out with a thermogravimetric analyzer that consists of an electronic microbalance surrounded by a furnace. The microbalance records any mass change as the temperature of the sample is being increased. The weight of the sample is plotted as a function of temperature for experiments carried out at a constant heating rate. This technique is widely used to monitor thermal stability and the loss of volatile components for materials where a loss of mass occurs because of thermal degradation or desolvation (the removal of solvent from a material). [33]

4. Experimental section

4.1. Synthesis of radical adduct 1*

The ensemble of reactions, without taking in account each synthesis path individually, is exposed as a list in the following chapter.

4.1.1. Synthesis of tris(2,4,6-trichlorophenyl)methyl radical (TTM)

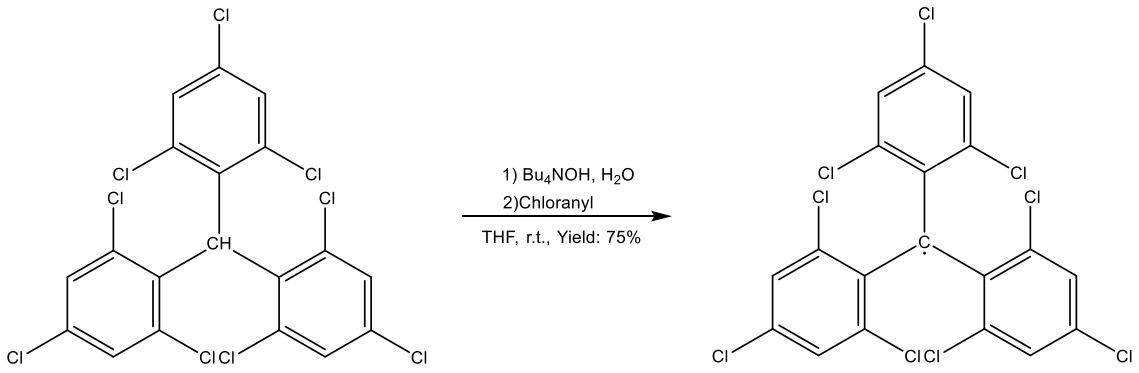

Fig. 21. αHTTM radicalization.

TTM radical was obtained from a mixture of αHTTM (5 g, 9.0 mmol), which was already synthesized, tetrahydrofuran (THF) (100 mL) and tetrabutylammonium hydroxide (TBAOH) (1.5 M, 8 mL). Then, it was stirred at room temperature under an Ar_2 atmosphere in the dark for 4 hours. Once it was completed, chloranil (3.2 g, 13.0 mmol) was added to the balloon and it was stirred for 45 minutes more under Ar_2 atmosphere. The reaction mixture was poured into diluted HCl and filtered. The precipitate was dried under vacuum and chromatographed in silica gel with hexane as eluent to get the radical adduct dissolved. Finally, hexane was concentrated at low pressure to obtain a red solid, TTM radical (3.75 g, 6.8 mmol). An IR was done to confirm it was TTM. Reaction yield: 75 % (Fig. 21).

IR (cm^{-1}): 1552 (m), 1520 (m), 1368 (m), 855 (s), 817 (m), 804 (s), 795 (s), (see Fig. A.1).

4.1.2. Synthesis of 3,6-dinitro-9*H*-carbazole (3,6-NO_2Cz)

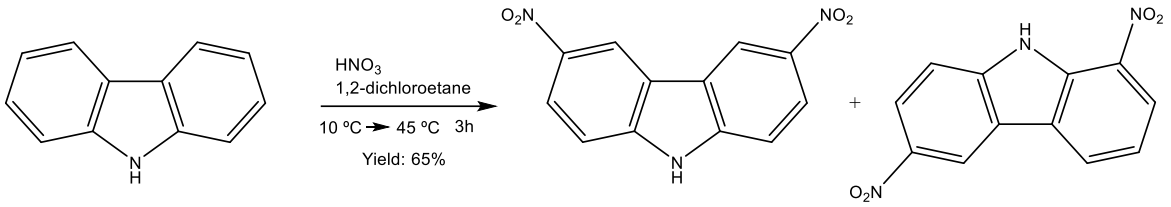

Fig. 22. Carbazole nitration.

Carbazole (5.01 g, 30 mmol) was dissolved in 1,2-dichloroethane (100 mL) an stirred under anhydride atmosphere, surrounded with ice, until it was cooled to 10 ºC. Then, a mixture of HNO_3 and 1,2-dichloroethane (1:1, 7.3 mL each) was added dropwise. Next, it was warmed at 45 ºC and stirred for 3.5 hours still under anhydride atmosphere. When the reaction was finished, the balloon content was filtered and dried under vacuum. This product was a mixture of two isomers: 1,6-dinitro-*9H*-carbazole (1,6-NO_2Cz) and 3,6-NO_2Cz (Fig. 22).

In order to pull them apart, two different ways were tried:

- In first one, the product was dissolved into a mixture of $CHCl_3$ and EtOAc, warmed and filtered, because a fraction of the product was not soluble. Then, a TLC was done to both fraction to know if one of them was pure. As the result was not the expected one, both fractions were mixed again and concentrated to obtain the initial solid product.

- The second one consisted in dissolving the product with KOH (25 g), water (315 mL) and EtOH (315 mL). Then, it was filtered (the solid part, which was brown, was the 1,6-NO_2Cz) and the dissolution was acidified with HCl in order to make it precipitate again. This second precipitate, a light brown solid, was the 3,6-NO_2Cz so it was filtered, washed with water and dried under vacuum. To identify both of them, ^{1}H-NMR an IR was done. Reaction yield: 3,6-NO_2Cz (65 %), 1,6-NO_2Cz (23 %).

^{1}H NMR (400 MHz, DMSO-d_6): δ (ppm) 7.46 (t, *J* = 7.9 Hz, 1H), 7.84 (d, *J* = 9.0 Hz, 1H), 8.34 – 8.41 (m, 2 H), 8.84 (d, J = 7.6 Hz, 1 H), 9.26 (s, 1 H), 12.68 (s, 1H), (**1,6-NO_2Cz**), (see Fig. A.2).

^{1}H NMR (400 MHz, DMSO-d_6): δ (ppm) 7.8 (d, *J* = 9.0 Hz, 2H), 8.4 (dd, *J* = 9.0, 2.3 Hz, 2H), 9.50 (d, *J* = 2.3 Hz, 2H), 12.8 (s, 1H), (**3,6-NO_2Cz**), (see Fig. A.3).

IR (cm^{-1}): **1,6-NO_2Cz**: 3422 (s), 3383 (m), 3092 (w), 1522 (m), 1483 (m), 1332 (s), 1286 (s), 1220 (m), 1204 (s), 1182 (m), 1100 (m); **3,6-NO_2Cz**: 3396 (m), 3342 (m), 3089 (w), 1607 (m),

1510 (m), 1473 (m), 1327 (s), 1306 (s), 1238 (m), 1104 (m), 812 (m), 751 (m), 717 (m), (see Fig. A.4 and Fig. A.5 respectively).

Synthesis of [4-(3,6-dinitro-9*H*-carbazolil)-2,6-dichlorophenyl]bis(2,4,6-trichlorophenyl)methane (αHNO$_2$CzTTM)

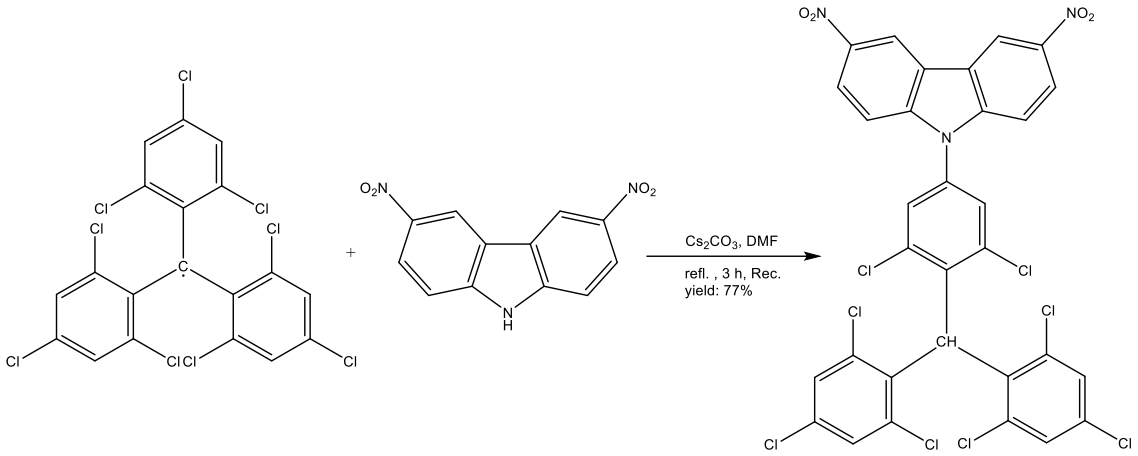

Fig. 23.TTM and 3,6-NO$_2$Cz coupling reaction.

A mixture of TTM (501 mg, 0.9 mmol), 3,6-NO$_2$Cz (955 mg, 3.7 mmol), anhydrous Cs$_2$CO$_3$ (542 mg, 1.7 mmol) and DMF (11 mL) was stirred at reflux for 3 hours in an inert atmosphere of Ar$_2$ at 150 ºC in the dark. Once it was cooled down, it was poured into an excess of diluted aqueous HCl acid to make the product precipitate. Then, it was filtered off and dried under vacuum. To see if the reaction was successfully completed, a TLC was done. The result showed that the coupling was not successful. Nevertheless, in order to recover 3,6-NO$_2$Cz and αHTTM from the mixture produced, a solution of CHCl$_3$ with the product was stirred at reflux for 45 min. Then, it was filtered off and dried again. The insoluble part was 3,6-NO$_2$Cz (0.74 g, 2.9 mmol) and the soluble part was chromatographed in silica gel with a solution of hexane and EtOAc to obtain αHTTM, a red solid (0.35 g, 0.6 mmol). IR was done to identify both of them. Recovery yield: 3,6-NO$_2$Cz (77 %), αHTTM (71 %) (Fig. 23).

IR (cm^{-1}): **3,6-NO$_2$Cz**: 1514 (m), 1476 (m), 1330 (s), 1305 (s), 1241 (m), 1102 (m), 813 (m), 752 (m), 718 (m), 666 (m); **αHTTM**: 1571 (m), 1540 (m), 1366 (m), 897 (m), 854 (s), 818 (m), 802 (s), 565 (m), (see Fig. A.6 and Fig. A.7 respectively).

4.1.3. Synthesis of [4-9*H*-carbazolyl-2,6-dichlorophenyl]bis(2,4,6-trichlorophenyl)methane (αHCzTTM)

This synthesis is divided in two steps: the first one consists on a coupling reaction and the second one is a reduction of the product obtained because it is a mixture of αH and radical.

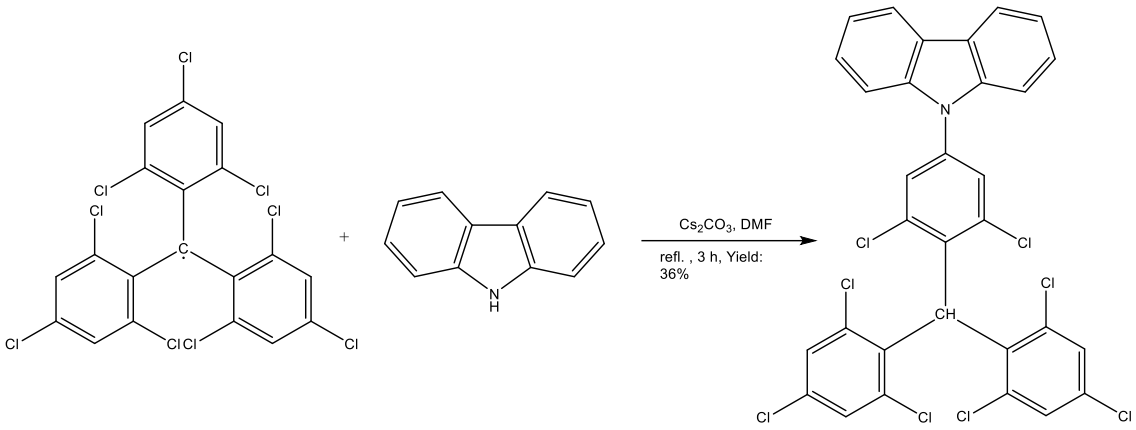

Fig. 24. TTM and carbazole coupling reaction.

1) A mixture of TTM (505 mg, 0.9 mmol), carbazole (623 mg, 3.7 mmol), anhydrous Cs_2CO_3 (549 mg, 1.7 mmol) and DMF (10 mL) was stirred at reflux for 3 hours in Ar_2 atmosphere at 155 ºC in the dark. Once it was cooled down, it was poured into an excess of diluted aqueous HCl acid to make the product precipitate. Then, it was filtered off and dried under vacuum. This product was a mixture of αHCzTTM - CzTTM (mostly αH product), αHTTM (precursor without coupling but gaining hydrogen) and other derivatives (TTM bounded to more than one carbazole). In order to purify it, on one hand, a chromatography in silica gel with hexane as eluent was done to get αHTTM. Then, on the other hand, as αHCzTTM - CzTTM is more polar than αHTTM, the eluent was changed to hexane (80 %)/$CHCl_3$ (20 %). Finally, both were concentrated at low pressure to obtain solid αHTTM (235 mg, 0.4 mmol) and αHCzTTM - CzTTM, a brown solid (209 mg, 0.3 mmol). IR was done to identify both of them. Reaction yield: αHTTM (47 %), αHCzTTM - CzTTM (34 %) (Fig. 24).

   This reaction was repeated with the following quantities: TTM (701 mg, 1.3 mmol), carbazole (870 mg, 5.2 mmol), anhydrous Cs_2CO_3 (552 mg, 1.7 mmol) and DMF (13 mL). The results obtained were: αHTTM (293 mg, 0.5 mmol) and αHCzTTM - CzTTM (316 mg, 0.5 mmol). Reaction yield: αHTTM (42 %), αHCzTTM - CzTTM (36 %).

   IR (cm^{-1}): **αHTTM**: 1574 (m), 1541 (m), 1367 (m), 898 (m), 855 (s), 844 (m), 818 (m),

802 (s), 780 (m), 768 (m), 567 (m). **αHCzTTM - CzTTM**: 1540 (m), 1464 (m), 1370 (m), 1232 (m), 860 (m), 808 (m), 746 (s), 722 (s), 565 (m), (see Fig. A.8 and Fig. A.9 respectively).

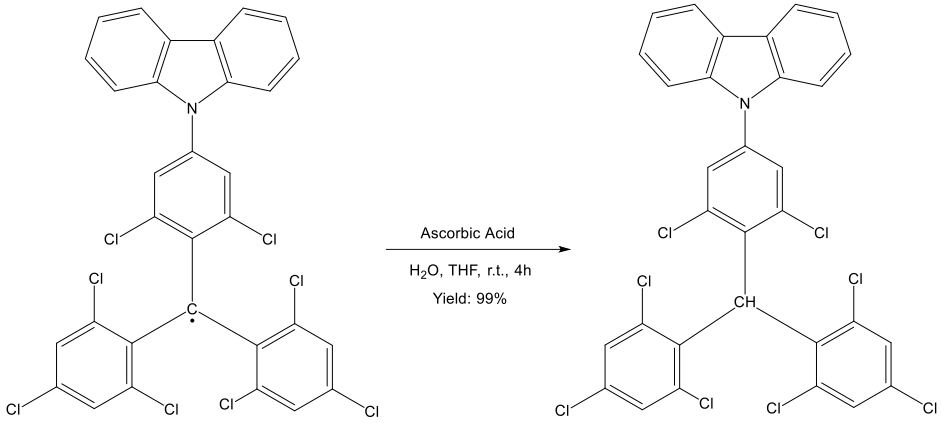

Fig. 25. CzTTM reduction.

2) A mixture of coupling product (mostly αHCzTTM) (439 mg, 0.6 mmol), ascorbic acid (442 mg, 2.5 mmol) and a solution of THF with distilled water (20 mL, 2 mL) was stirred for 4 hours at room temperature. As the mixture continued having a strong brown colour, the reaction was not finished yet (the αHCzTTM is less colourful) so some HCl was added to improve the protonation. Then, it was poured into distilled water. In order to obtain the light brown precipitate, a liquid-liquid extraction with $CHCl_3$ was done and after it was concentrated at low pressure. An IR was done to confirm it was αHCzTTM. Reaction yield: 99 % (Fig. 25).

IR (cm^{-1}): 1541 (m), 1463 (m), 1453 (m), 1227 (m), 857 (m), 804 (m), 746 (s), 723 (m), (see Fig. A.10).

4.1.4. Synthesis of [4-(3,6-dinitro-9*H*-carbazolyl)-2,6-dichlorophenyl]bis(2,4,6-trichlorophenyl)methyl radical (NO_2CzTTM)

This reaction is divided in two steps, CzTTM nitration and radicalization of the resulting product:

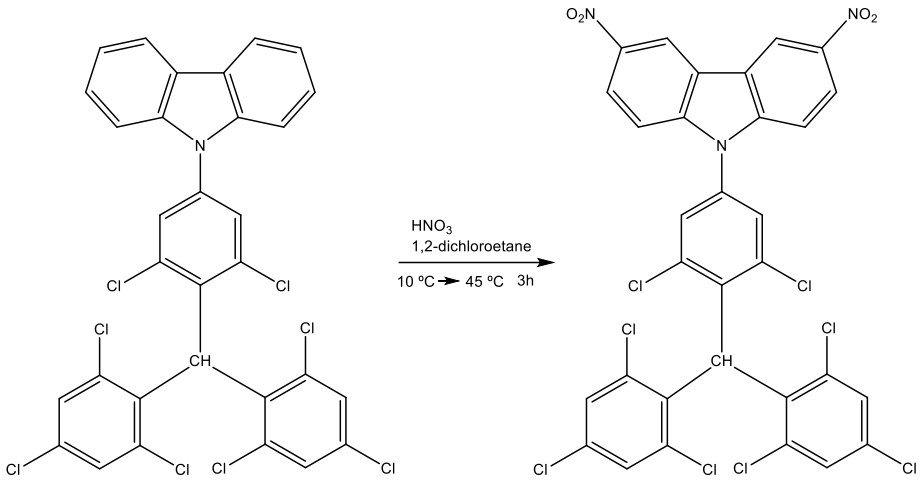

Fig. 26. αHCzTTM nitration.

1) αHCzTTM (435 mg, 0.6 mmol) was dissolved in 1,2-dichloroethane (11 mL) an stirred under anhydride atmosphere, surrounded with ice, until it was cooled to 10 ºC. Then, a mixture of HNO_3 and 1,2-dichloroethane (1:1, 0.19 mL each) was added. Next, it was warmed at 45 ºC and stirred for 3.5 hours still under anhydride atmosphere (Fig. 26). When the reaction was finished, the balloon content was filtered and dried under vacuum. A TLC was done with $CHCl_3$ (80 %)/hexane (20 %). The results showed that the product was pure enough (with some insignificant impurities).

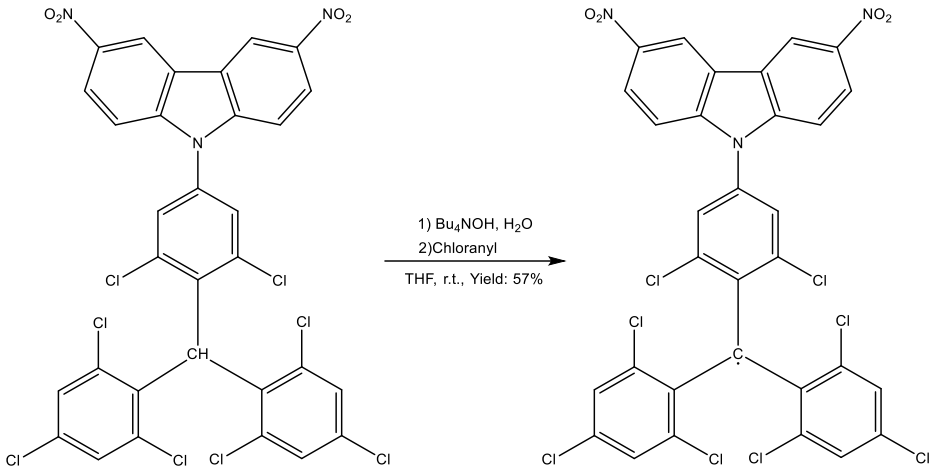

Fig. 27. αHNO₂CzTTM radicalization.

2) NO_2CzTTM was obtained from a mixture of αHNO_2CzTTM (365 mg, 0.5 mmol), THF (20 mL) and TBAOH (1.5 M, 0.41 mL). This was stirred at room temperature under an Ar_2 atmosphere in the dark for 4 hours. Once it was completed, chloranil (162 mg, 0.7 mmol) was added to the balloon and it was stirred for 45 minutes more under Ar_2 atmosphere. The reaction mixture was poured into diluted HCl, filtered and dried under vacuum. In order to purify it, $CHCl_3$ was added to the solid, it was filtered and two different fractions were pulled off. The insoluble part, a red solid, was analysed with IR and ESI-HRMS and was identified as NO_2CzTTM. The soluble part was concentrated at low pressure and the solid was chromatographed in silica gel with hexane/$CHCl_3$ as eluent to get the purified product. It was found out it was a subproduct from nitration reaction. Instead of having two nitro groups, it only had one (IR and ESI-HRMS analysis too). The results obtained were: NO_2CzTTM (0.28 g, 0.4 mmol) and monoNO_2CzTTM (0.03 g, 0.05 mmol); Reaction yield: NO_2CzTTM (57 %), monoNO_2CzTTM (7 %) (Fig. 27).

ESI-HRMS: calculated for $C_{31}H_{12}{}^{35}Cl_8N_3O_4$ 769.8342, found (*m/z)* 769.8332; calculated for $C_{31}H_{13}{}^{35}Cl_8N_2O_2$ 724.8491, found (*m/z)* 724.8499. (see Fig. A.11 and Fig. A.12 respectively).

IR (cm^{-1}): **NO_2CzTTM**: 1509 (m), 1334 (s), 1286 (s), 1232 (m), 856 (m), 820 (m), 799 (m), 750 (m), 719 (m); **monoNO_2CzTTM:** 1514 (m), 1334 (s), 1308 (m), 856 (m), 813 (m), 797 (s), 746 (s), 719 (m), (see Fig. A.13 and Fig. A.14 respectively).

4.1.5. Synthesis of 3,6-diamino-9*H*-carbazole (3,6-NH_2Cz)

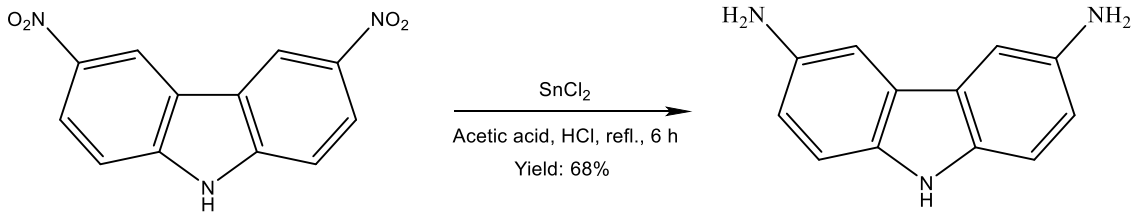

Fig. 28. 3,6-NO_2Cz reduction.

3,6-NO_2Cz (301 mg, 1.2 mmol) was mixed with anhydrous $SnCl_2$ (2.21 g, 11.7 mmol) in AcOH (3 mL) and HCl (10 mL) under Ar_2 atmosphere. The mixture was stirred at reflux for 6 hours. The reaction mixture was cooled down to room temperature, filtered and the precipitate was re-dissolved with water. After that, 20 % NaOH was added and filtered the occurred precipitate. Then, it was collected by filtration, washed with water and dried under vacuum to obtain the product as a black solid (0.16 g, 0.8 mmol) An IR was done to identify the product. Reaction yield: 68 % (Fig. 28).

This reaction was repeated with the following quantities: 3,6-NO_2Cz (1.07 g, 3.9 mmol), anhydrous $SnCl_2$ (7.32 g, 38.6 mmol), AcOH (6 mL) and HCl (32 mL). The product obtained was 0.50 g (2.5 mmol) of 3,6-NH_2Cz. Reaction yield: 64 %.

IR (cm^{-1}): 3383 (w), 3186 (w), 3014 (w), 1466 (m), 867 (m), 762 (m), 734 (m), 684 (m), 584 (s), (see Fig. A.15).

4.1.6. Synthesis of [4-(3,6-diamino-9*H*-carbazolyl)-2,6-dichlorophenyl]bis(2,4,6-trichlorophenyl)methane (αHNH$_2$CzTTM)

This compound was tried to be synthesized by two different ways, by reduction and coupling reactions. The reduction reaction was tried twice with different methodologies:

Option 1:

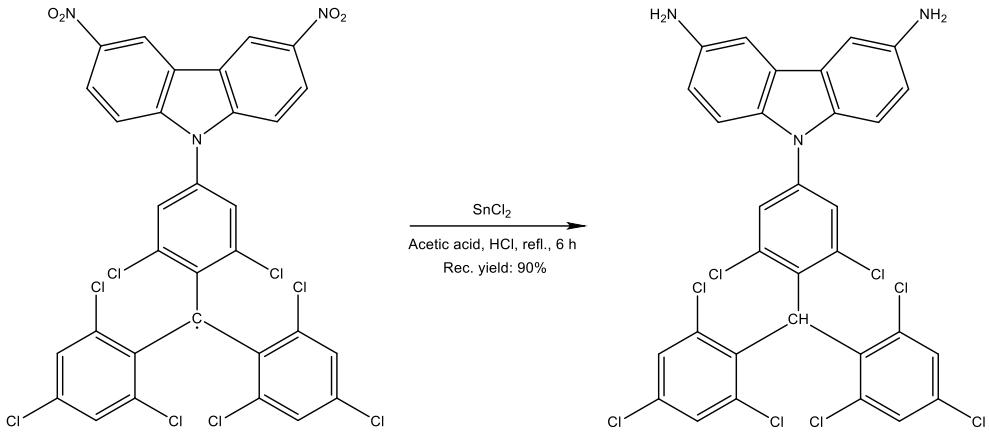

Fig. 29. NO_2CzTTM reduction option 1.

NO_2CzTTM (250 mg, 0.3 mmol) was mixed with anhydrous $SnCl_2$ (0.61 g, 3.2 mmol) in AcOH (2.6 mL) and HCl (13.8 mL) under Ar_2 atmosphere. The mixture was stirred at reflux for 6 hours. The reaction mixture was cooled down to room temperature, filtered, cleaned with a solution of 20 % NaOH and cleaned again with distilled water. It was dried under vacuum and an IR was done. The results showed that the product, a red solid, was NO_2CzTTM indeed (0.23 g, 0.2 mmol). Recovery yield: 90 % (Fig. 29).

IR (cm^{-1}): 1509 (m), 1334 (s), 1286 (s), 1232 (m), 856 (m), 820 (m), 800 (m), 750 (m), 719 (m), (see Fig. A.16).

Option 2:

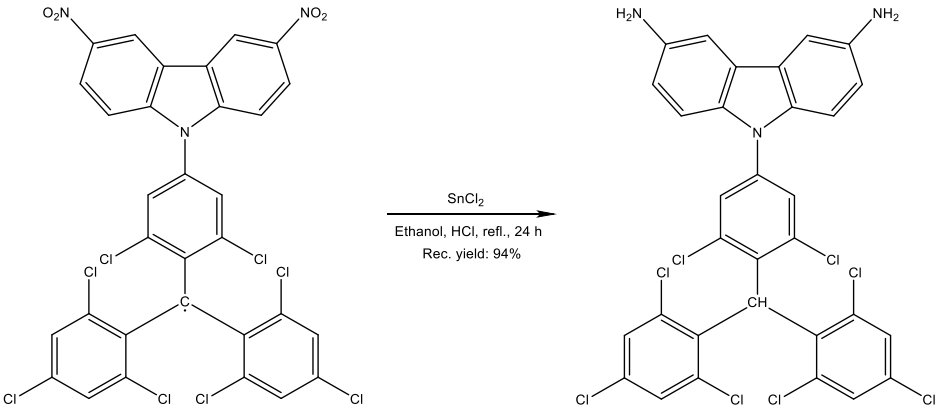

Fig. 30. NO_2CzTTM reduction option 2.

NO_2CzTTM (220 mg, 0.3 mmol) was mixed with anhydrous $SnCl_2$ (0.22 g, 1.2 mmol) in EtOH (20 mL) and HCl (2 mL) under Ar_2 atmosphere. The mixture was stirred at reflux for 22 hours. The reaction mixture was poured into an excess of water, filtered, cleaned with distilled water and dried under vacuum. Finally, an IR was done. The results showed that the product was NO_2CzTTM again (0.21 g, 0.3 mmol). Recovery yield: 94 % (Fig. 30).

IR (cm^{-1}): 1509 (m), 1334 (s), 1286 (s), 1233 (m), 856 (m), 820 (m), 800 (m), 750 (m), 719 (m), (see Fig. A.17).

The coupling reaction was the following one:

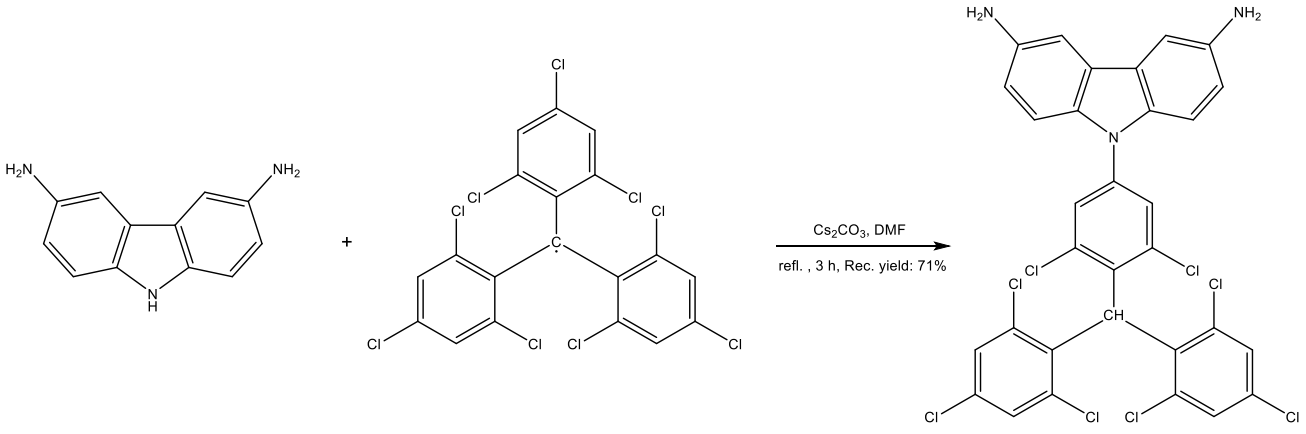

Fig. 31. 3,6-NH_2Cz and TTM coupling reaction.

A mixture of TTM (482 mg, 0.9 mmol), 3,6-NH_2Cz (203 mg, 1.0 mmol), anhydrous Cs_2CO_3 (485 mg, 1.5 mmol) and DMF (10 mL) was stirred to reflux for 3 hours in an inert atmosphere of Ar_2 at 153 ºC in the dark. Once it was cooled down, it was poured into an excess of diluted aqueous HCl acid to make the product precipitate. Then, it was filtered off and the acid water was kept for further neutralization with $NaHCO_3$. The solid product was cleaned up with water but after seeing that it was slightly soluble on it, a liquid extraction with $CHCl_3$ was done. The soluble part (0.34 g) was a brown solid and the insoluble one (0.03 g) was a black solid. Finally, the neutralized acid solution was filtered off and a black precipitate (0.13 g) was dried under vacuum. An IR was done for the three different parts but only the soluble part was identified (αHTTM). None of the other solids was the expected product leading to conclude the reaction was unsuccessful. Recovery yield: 71 % (Fig. 31).

IR (cm^{-1}): **Soluble part (αHTTM)**: 1574 (m), 1541 (m), 1367 (m), 898 (m), 855 (m), 802 (s), 780 (m), 768 (m), 567 (m); **Insoluble part**: 1423 (s), 878 (m), 803 (m); **Acid water solid**: 1502 (m), 1467 (m), 1332 (m), 1220 (m), 867 (m), 805 (m), 586 (s), (see Fig. A.18, Fig. A.19 and Fig. A.20 respectively).

4.2. Synthesis of radical adduct 2*

This synthesis is divided in two steps: the coupling of tris(2,3,5,6-tetrachlorophenyl)methyl radical (DTM) with 3,6-dibromo-9*H*-carbazole (3,6-BrCz), and the further radicalization of it:

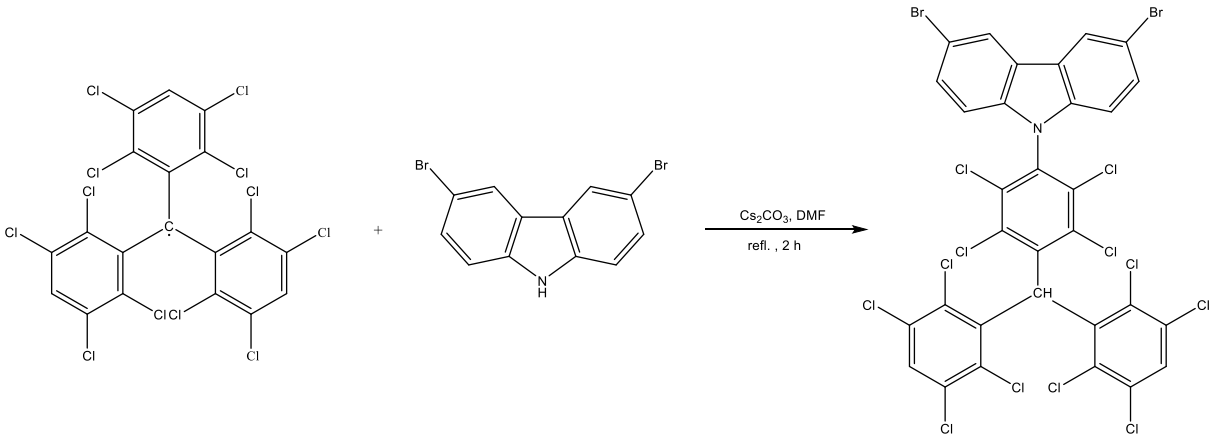

Fig. 32. 3,6-BrCz and DTM coupling reaction.

1) A mixture of DTM (500 mg, 0.8 mmol), which was already synthesized, 3,6-BrCz (330 mg, 1.0 mmol), anhydrous Cs_2CO_3 (570 mg, 1.8 mmol) and DMF (5 mL) was stirred at reflux for 3 hours in an inert Ar_2 atmosphere at 150 ºC in the dark. Once it was cooled down, it was poured into an excess of diluted aqueous HCl acid to make the product precipitate. Then, it was filtered and dried under vacuum. In order to obtain a pure product, a chromatography in silica gel with hexane as eluent was done to get αHDTM.

Next, eluent was changed for hexane (80 %)/$CHCl_3$ (20 %) and the supposed αHBrCzDTM was obtained. Both solution were concentrated at low pressure to obtain an orange solid (315 mg, 0.5 mmol) and a dark lilac solid (301 mg, 0.3 mmol) respectively. An IR was done to confirm that the first product from the column was αHDTM (Fig. 32).

IR (cm^{-1}): 1410 (m), 1386 (s), 1163 (s), 1098 (m), 865 (s), 844 (m), 781 (m), 704 (s), 688 (m), 646 (m), 625 (s), (see Fig. A.21).

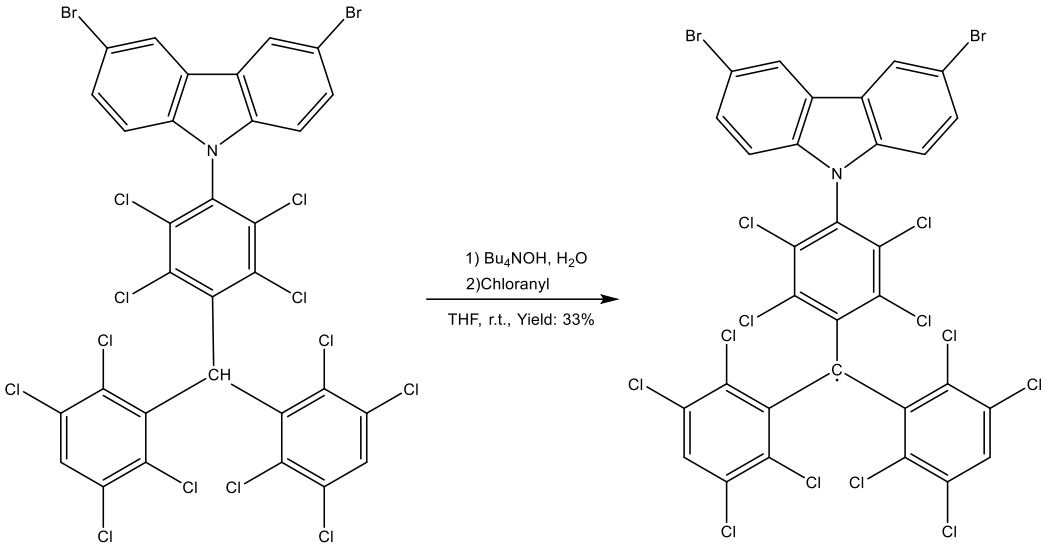

Fig. 33. αHBrCzDTM radicalization.

2) BrCzDTM radical was obtained from a mixture of αHBrCzDTM (0.30 g, 0.3 mmol), THF (15 mL) and TBAOH (1.5 M, 0.3 mL). This was stirred at room temperature under an Ar_2 atmosphere in the dark for 4 hours. Once it was completed, chloranil (106 mg, 0.4 mmol) was added to the balloon and it was stirred for 45 minutes more under Ar_2 atmosphere (Fig. 33). The reaction mixture was poured into diluted HCl and filtered. The precipitate was dried and chromatographed in silica gel with hexane as eluent to get the radical adduct dissolved in it. Finally, it was concentrated at low pressure to obtain a black red solid, BrCzDTM radical (**2**$^{\bullet}$) (248 mg, 0.3 mmol). IR and ESI-HRMS were done to identify it. Reaction yield: 33 %. Radical purity: 98 % (magnetic susceptibility analysis).

IR (cm^{-1}): 1470 (m), 1437 (m), 1380 (m), 1230 (m), 1172 (m), 804 (s), 722 (m), 707 (m), 638 (m), (see Fig. A.22).

ESI-HRMS: calculated for $C_{31}H_8Br_2{}^{35}Cl_{12}N$ 971.5291, found (*m/z)* 971.5314. On Fig. 34 these results are showed.

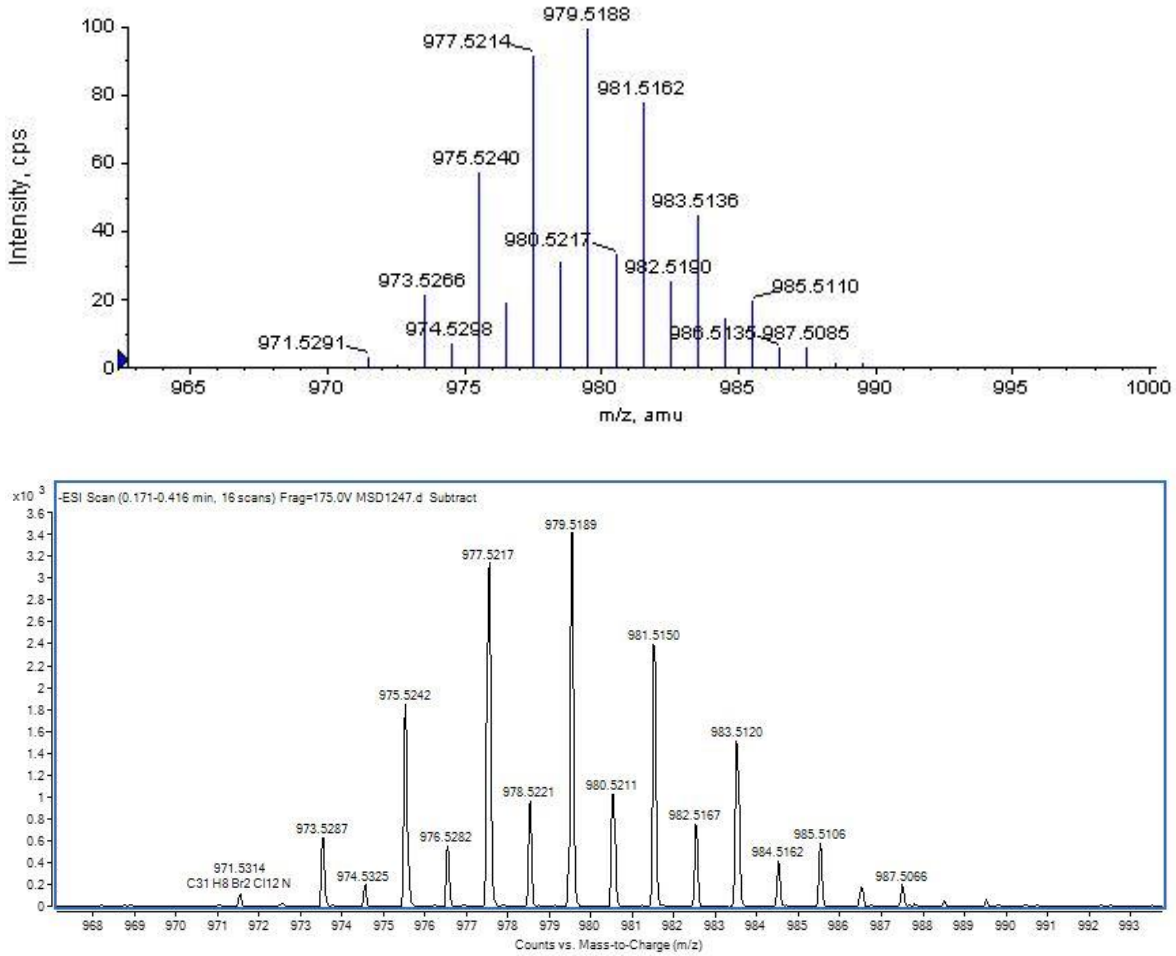

Fig. 34.ESI-HRMS analysis for 2. It is shown chlorine isotopic distribution. On the top, theoretical one, and on the bottom, the experimental distribution.*

4.3. Characterization

As it was said on previous chapters, characterization techniques have been done only for radical adduct **2*** because **1*** was not possible to synthesize. In this chapter, it is explained the experimental methodology followed in each analysis in order to be replicable. Only from three techniques will be explained the methodology, which are UV-Vis, EPR and CV.

4.3.1. UV-Visible Spectroscopy

This technique have been carried out at Institut de Química Avançada de Catalunya (IQAC-CSIC) with a Varian Cary 3000 Bio Spectrophotometer, using a quartz cuvette with an optical path of 1 cm.

The procedure was divided in two parts:

- Sample preparation: 0.6 and 1.1 mg of product was weighted and introduced into a volumetric flask (10 mL or 25 mL). Then, a solution was prepared with a specific solvent. On Table 1 is shown the list of samples prepared.

- Sample analysis: Before analysing any sample, it was done a blank with only the solvent (because it has its own absorbance too). Hence, the difference between the two trials was due to radical adduct **2***.

	Solvent	Mass (mg)	Volume (mL)	Concentration (M)
Sample 1	C_6H_{12}	1	10	10^{-4}
Sample 2	Toluene	0.9	10	$9x10^{-5}$
Sample 3	DCM	0.7	10	$7x10^{-5}$
Sample 4	$CHCl_3$	0.8	10	$8x10^{-5}$
Sample 5	THF	0.7	10	$7x10^{-5}$
Sample 6	EtOAc	0.8	10	$8x10^{-5}$
Sample 7	Acetone	0.6	10	$6x10^{-5}$

	Solvent	Mass (mg)	Volume (mL)	Concentration (M)
Sample 8	$CHCl_3$	0.9	10	$3x10^{-4}$
Sample 9	$CHCl_3$	1.1	25	$5x10^{-5}$
Sample 10	$CHCl_3$	0.9	10	10^{-4}
Sample 11	$CHCl_3$	0.6	25	$4x10^{-5}$

Table 1. Sample details prepared for UV-Vis analysis.

Table 1 describes in detail the characteristics of each sample. From sample 1 to 7, radical adduct **2*** is analysed with different solvents. At the beginning, **2*** was difficult to dissolve in both cyclohexane (C_6H_{12}) and acetone, but warming it a little bit helped to dissolve it completely.

Samples 8 and 9 were a solution of chloroform with the pure electron-donor moiety from **2***, 3,6-BrCz. The same happens with samples 10 and 11, which were a solution of chloroform with the pure electron-acceptor moiety from **2***, DTM radical. As it will be explained on results chapter, samples 8 and 10 were too concentrated. Owning to that fact, samples 9 and 11 were done with more solvent volume.

4.3.2. Electron Paramagnetic Resonance (EPR)

EPR radical adduct characterization was carried out at IQAC-CSIC with a spectrometer EMX of Bruker (Fig. 35), with a microwave bridge of X-band (~9 GHz) EMX premium X, magnet of 10" ER073 with a power supply of 12 KW ER083.

As it is necessary to use anhydrous solvent to work with the EPR technique, a DCM distillation with $CaCl_2$ was done. Then, 1.1 mg of **2*** was weighted and dissolved with 1 mL of DCM in a 4 mL glass vial ($1.12x10^{-3}$ M). Once it was completely dissolved, the solution was introduced into a thin quartz tube for further analysis. The analysis was done at room temperature (298 K) and at 223 K.

Fig. 35. Bruker EMX spectrometer from IQAC-CSIC facilities. [34]

4.3.3. Cyclic Voltammetry

This characterization was carried out at the organic chemistry department of Universitat de Barcelona (UB). The instrumental used was a potentiostat/galvanostat *Eco Chemie Autolab PGSTAT30* equipped with *GPES* software. The electrochemical cell was formed by a an Ag/Ag^+ ($AgNO_3$ 1mM in CH_3CN) reference electrode (RE), a glassy carbon working electrode (WE) and a platinum wire as counter electrode (CE). The supporting electrolyte was tetrabutylammonium hexafluorophosphate (0.1 M) and the solution (0.5 mM) was prepared with DCM.

Inevitably, oxygen undergoes a reversible one-electron reduction to form the oxygen radical anion (superoxide, $O_2^{\bullet -}$) leading to use an inert atmosphere of argon for sparging the solution before measurements are taken. In addition, to continue guarantying the inert atmosphere, the Teflon tubing used for sparging is placed above the surface of the solution during data collection.

The first traces were recorded with a scan rate of 100 mV/s either on negative and positive potentials (reduction and oxidation part respectively). Then, if the process seemed reversible, it was repeated at different scan rates to ensure electrochemical reversibility.

5. Results and discussion

5.1. UV-Visible spectroscopy characterization of radical adduct 2*

Table 2 presents the result of UV-Visible spectroscopy for samples 1 to 7 from Table 1. The values written are wavelength and molar absorptivity, λ(ε) in nm ($M^{-1}cm^{-1}$), of the UV-Vis spectrum of **2***.

C_6H_{12}	Toluene	DCM	$CHCl_3$	THF	EtOAc	Acetone
264 (20 250)	-	264 (27 570)	263 (21 350)	265 (23 260)	262 (21 380)	-
293 (16 090)	294 (14 120)	292 (20 140)	292 (16 270)	293 (17 040)	291 (16 160)	-
300 (20 710)	300 (17 240)	300 (23 100)	299 (19 870)	301 (20 680)	298 (19 340)	-
333 (8660)	333 (8230)	333 (9420)	332 (9090)	333 (9290)	331 (8770)	331 (8540)
347 (11 580)	348 (10 840)	349 (12 790)	347 (11 870)	349 (12 500) (SH)	347 (11 590)	347 (11 090)
363 (16 900) (SH)	-	363 (18 650) (SH)	365 (18 210) (SH)	364 (18 440)	363 (17 780)	362 (16 530)
378 (28 800)	379 (24 840)	378 (33 700)	378 (31 650)	378 (32 730)	376 (30 980)	377 (29 890)
493 (970)	492 (970)	509 (1230)	512 (1100)	507 (1150)	507 (1070)	508 (1080)
559 (1030)	557 (1010)	556 (1330)	558 (1210)	557 (1260)	557 (1190)	557 (1180)
621 (1100)	618 (930)	602 (1000)	611 (890)	605 (1017)	610 (870)	-

Table 2. Wavelength and molar absorptivity, λ(ε) in nm (M^{-1} cm^{-1}), of radical adduct samples.

Table 3 shows the values of wavelength and molar absorptivity of the UV-Vis spectra of 3,6-BrCz and DTM radical (samples 8-9 and 11 respectively).

Samples	Wavelength and molar absorptivity, λ(ε)
Sample 8-9 (3,6-BrCz)	268 (16 870), 302 (16 090), 335 (3290), 349 (2670), 378 (110)
Sample 11 (DTM)	265 (4080), 294 (3410) (SH), 332 (4520), 359 (12 450) (SH), 374 (23 980), 498 (790), 547 (640)

Table 3. Wavelength and molar absorptivity, λ(ε) in nm (M^{-1} cm^{-1}), of 3,6-BrCz and DTM.

These values exposed in both tables are taken from different peaks the spectrum showed. If a value was not clearly a peak because it was too close to another big maximum, then it was considered as a shoulder (SH).

The following figures (Fig. 36, Fig. 37, Fig. 38, Fig. 39) show UV-Vis spectra compared with different solvents or with different compounds. Then, they will be discussed in detail.

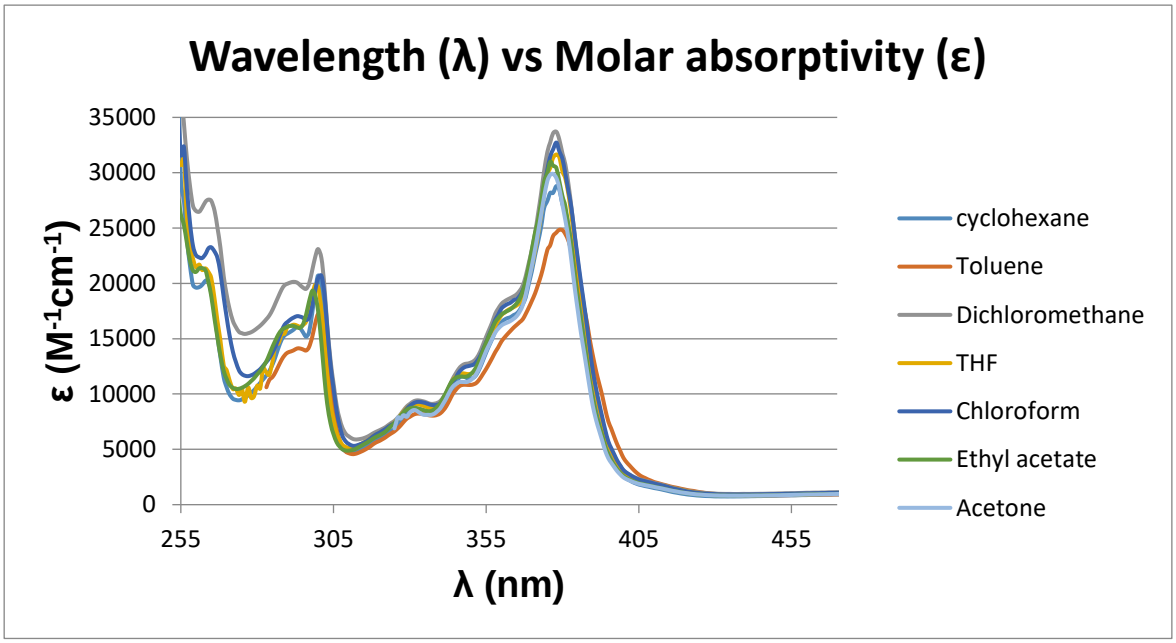

Fig. 36. UV-Vis spectrum of radical adduct 2 with different solvents. Range 255-470 nm.*

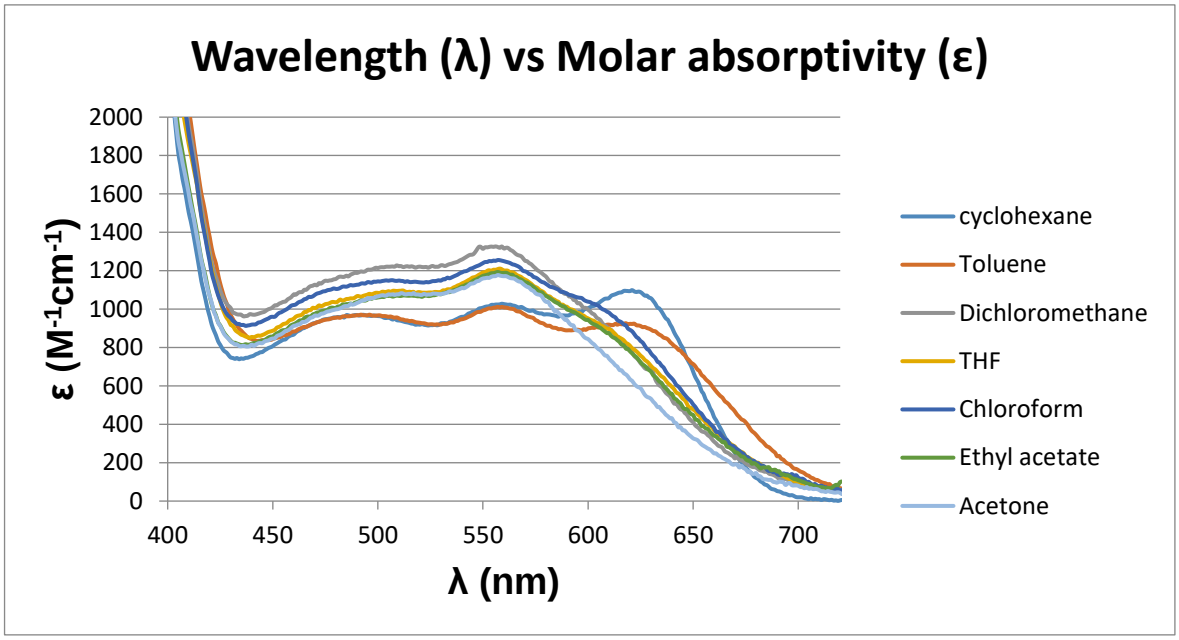

Fig. 37. UV-Vis spectrum of radical adduct 2 with different solvents. Range 400-720 nm.*

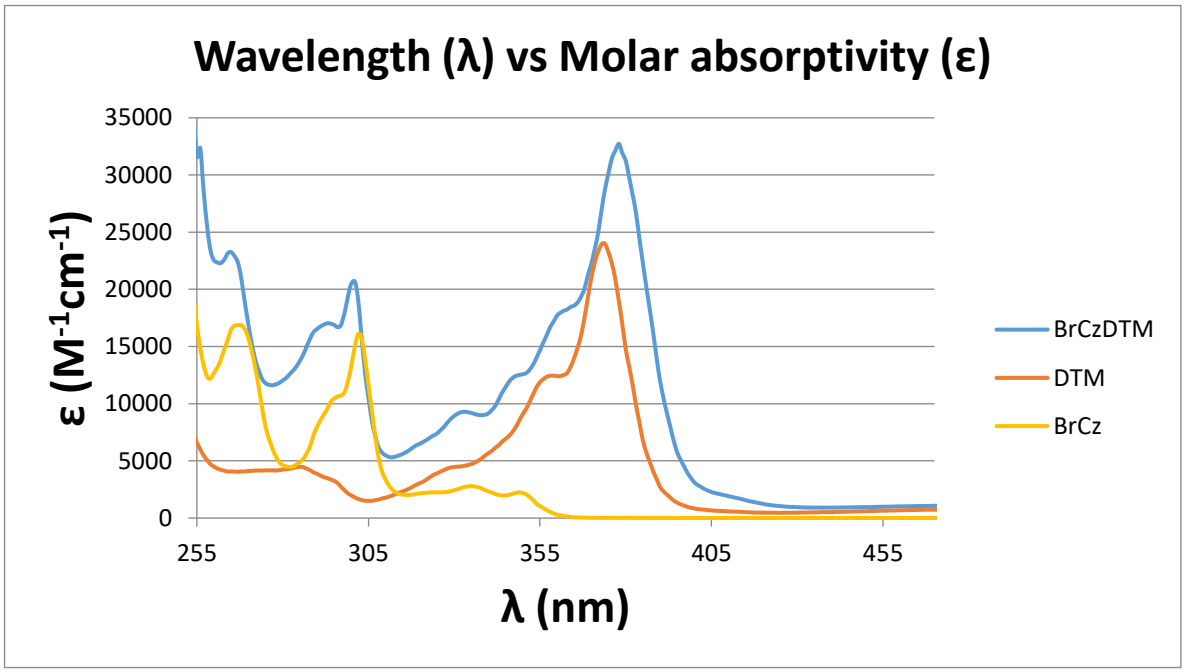

Fig. 38. UV-Vis spectrum comparison between 2 and its precursors with chloroform as solvent. Range 255-470.*

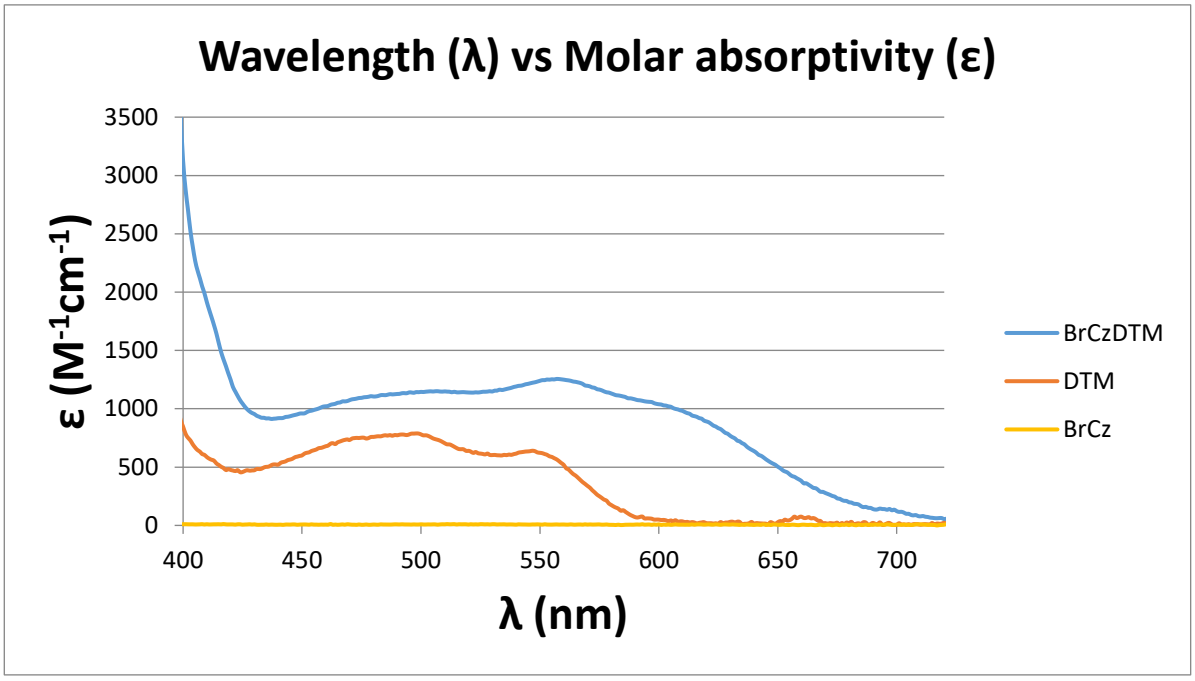

Fig. 39. UV-Vis spectrum comparison between 2 and its precursors with chloroform as solvent. Range 400-720.*

On the one hand, Fig. 36 and Fig. 37 illustrate UV-Vis spectrum of radical adduct **2*** among 255 and 720 nm. In addition, in both are represented all the solvents used despite the fact that, on the first figure, acetone and toluene at 320 and 290 nm respectively started to present oscillations. Moreover, looking carefully at these two absorption spectra, it can be observed that there is not any substantial difference between solvents, only hyperchromic and hypochromic shifts (increase and decrease of molar absorptivity respectively) among 255 and 600 nm. This leads to think the solvent does not affect electronic transitions.

However, the band between 600 and 650 nm is known as the charge-transfer band and as it can be seen, it moves depending on the solvent. Only in apolar solvents such as cyclohexane and toluene this band shifts to longer wavelengths. So, it can be said that polarity affects somehow to charge-transfer band. On the other hand, the spectral region in which this charge-transfer band appears is a function of the donor and/or acceptor strength of the redox centres in the molecule. This feature suggests a partial intramolecular electron transfer in the molecule from the donor, the 3,6-BrCz moiety, to the acceptor, the trivalent carbon. [10]

The charge-transfer band is the lowest energetic transition in the spectrum. This can be explained through a look into quantum chemistry, as a transition between HOMO from 3,6-BrCz moiety to LUMO from the trivalent carbon. [35]

On the other hand, Fig. 38 and Fig. 39 illustrate a comparison of absorption spectra between **2*** and its precursors among 255 and 720 nm. It can be said that bands between 255 and 315 nm, especially the one at 290 nm, on radical adduct **2*** are clearly due to 3,6-BrCz moiety because only this compound absorbs between this wavelength values. A similar situation happens with the absorption region from 370 to 600 nm because it is associated with the radical character of these compounds. Consequently, these bands can correspond to electronic configuration in the orbital from the unpaired electron, and the last band of the range can be related with molecule rigidity. The band at about 370 nm in **2*** is characteristic of the π → π* transition and have features similar to that of DTM radical corresponding to the triphenylmethyl moiety. [4]

5.2. EPR characterization of radical adduct 2*

The free electron in radical adduct **2*** can couple with different magnetic nuclei (in red colour on Fig. 40):

- Two hydrogens situated in *para* position respect the unpaired electron, with I = ½.

- Nitrogen atom from 3,6-BrCz moiety with I = 1.

-Carbon 13 (^{13}C) atom with I = ½. It can couple with the central carbon atom (C_α), three neighbouring carbon atoms (C_b), six *ortho* carbon atoms (C_0) and even with three *para* carbon atoms (C_p).

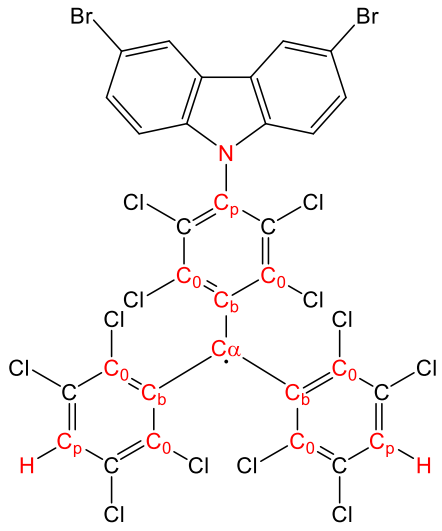

Fig. 40. Radical adduct 2 structure in detail. In red, there are marked different magnetic nuclei that can interact with the free electron.

Thus, as it can be seen from Table 4, that the further away is the magnetic nucleus from the

unpaired electron the smaller is the hyperfine coupling constant. Leading to this fact, it is deduced that majority of radical electronic spin density is capitalized by trivalent carbon followed by neighbouring carbons.

Parameter	298 K	223 K
g	2,00268	2,00268
a (H) (G)	1,85	1,8
a (N) (G)	-	-
a ($^{13}C_{\alpha}$) (G)	-	30,11
a ($^{13}C_{b}$) (G)	-	14,45
a ($^{13}C_{0}$) (G)	-	11,81
a ($^{13}C_{p}$) (G)	-	-
ΔH_{pp} (G)	1,34	1,07

Table 4. List of parameters deduced from EPR spectra analysis

Furthermore, Fig. 41 represents EPR spectrum of **2**$^{\bullet}$ at two temperatures.

The second column in Table 4, values at room temperature, shows the weak electron-coupling with two hydrogens as an overlapped triplet ($2 \cdot 2 \cdot \frac{1}{2} + 1 = 3$) (Fig. 41). Also, it can be detected in Fig. 41 some small peaks in the blue line between 3355 – 3368 G and 3383 – 3395 G. Those, which are zoomed in the red line, are due to electron-coupling with ^{13}C atoms. Specifically, the farthest with (3358 and 3392 G) are a result of C_{α} interaction and the shoulder at both sides of the central triplet signal is regarded as interaction with the three bridge-carbon atoms C_b.

The second one, produced at 223 K, shows more defined peaks as the linewidth (ΔH_{pp}) at 223 K is smaller than at 298 K (directly proportional to temperature, Table 4). In this case, it can be seen between 3365 – 3370 G and 3380 – 3385 G unpaired electron interaction with C_b and C_0 carbons (red line) but, unfortunately, they are overlapped. It is considered that the first peak after the shoulder is mainly due to C_0 interaction and the following one is a mixture of C_b and C_0 signals. In addition, interaction with C_p is not noticed in the spectrum, because if there is interaction, it is within the central triplet.

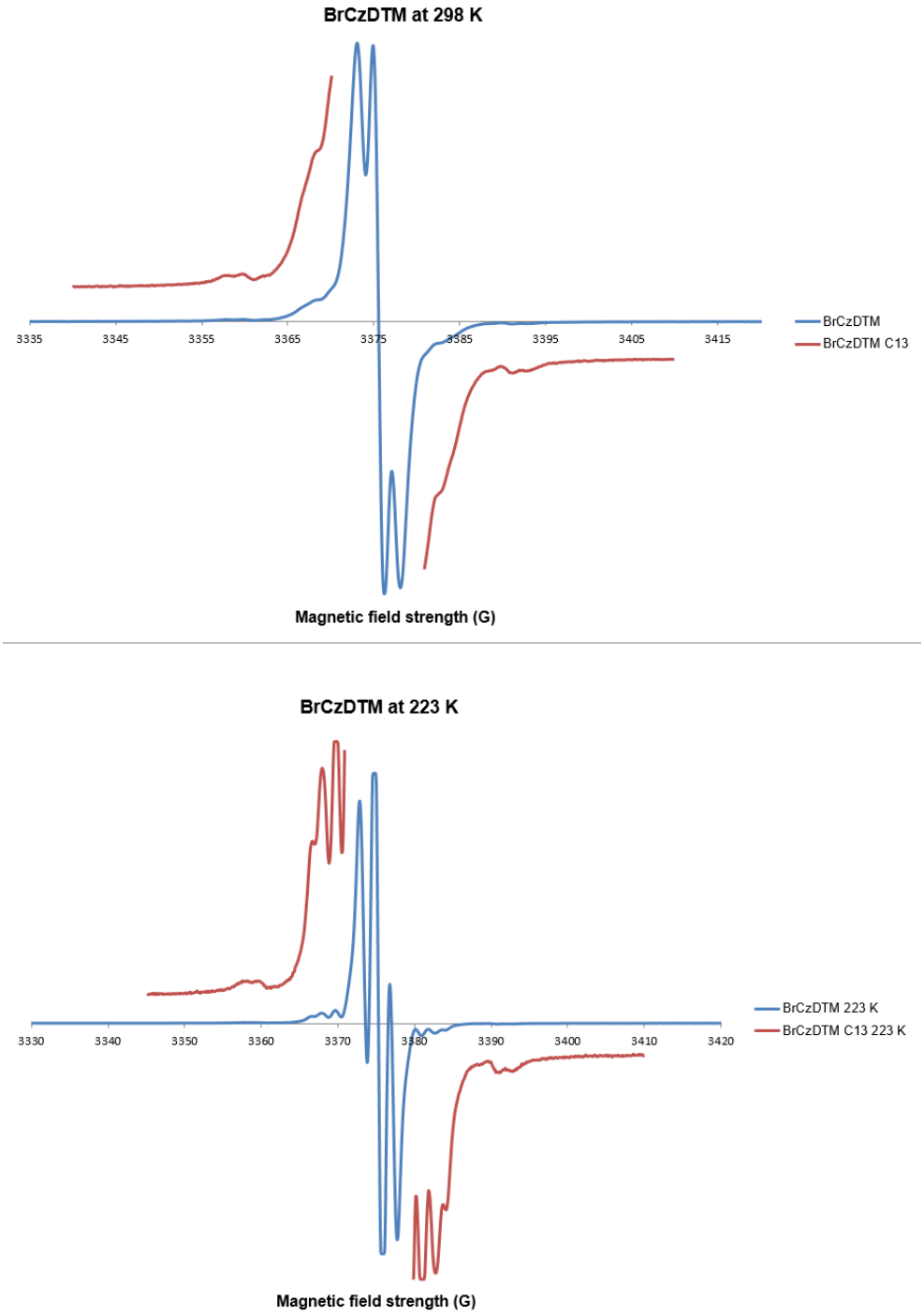

Fig. 41. On the top, EPR spectrum of 2* at 298 K. On the bottom, EPR spectrum of 2* at 223 K. The red line shows a zoom of 3355 – 3368 G and 3383 – 3395 G range.

Finally, to corroborate that calculated coupling values are correct, a simulation of EPR spectrum was done. Fig. 42 shows a comparison between simulated spectrum and the experimetal one at 223 K. Owning to the fact that are almost identical, it can be said that the values deduced from the experimental spectrum are correct.

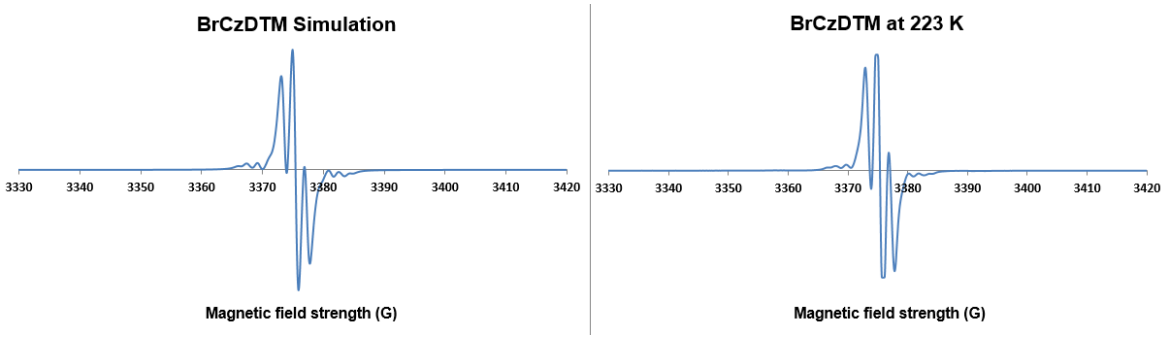

Fig. 42. On the left, EPR simulation. On the right, experimental spectrum at 223 K.

5.3. Cyclic voltammetry characterization of radical adduct 2*

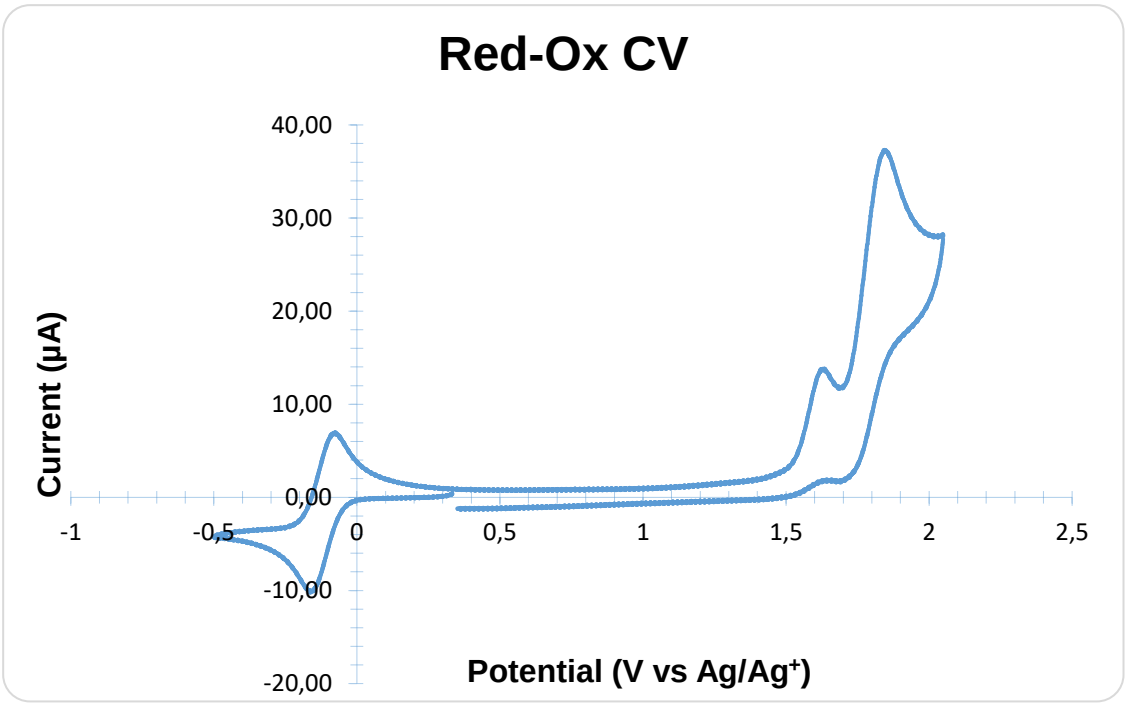

Fig. 43. Complete voltammogram of radical adduct 2. The left part conform reduction process and the right part conform the oxidation one.*

The cyclic voltammetry displayed one quasi-reversible redox pair, corresponding to its reduction (O_1/R_1), and an irreversible redox pair, coinciding to its oxidation (O_2/R_2). In the one hand, the quasi-reversible process is attributed to the equilibrium reaction involving the addition of one electron to the trivalent central carbon atom to form its stable anion. On the other hand,

the irreversible process is attributed to the removal of one electron from the trivalent central carbon atom to form its unstable cation, which is further oxidized as it can be seen on Fig. 43. Both redox processes are represented in Fig. 44.

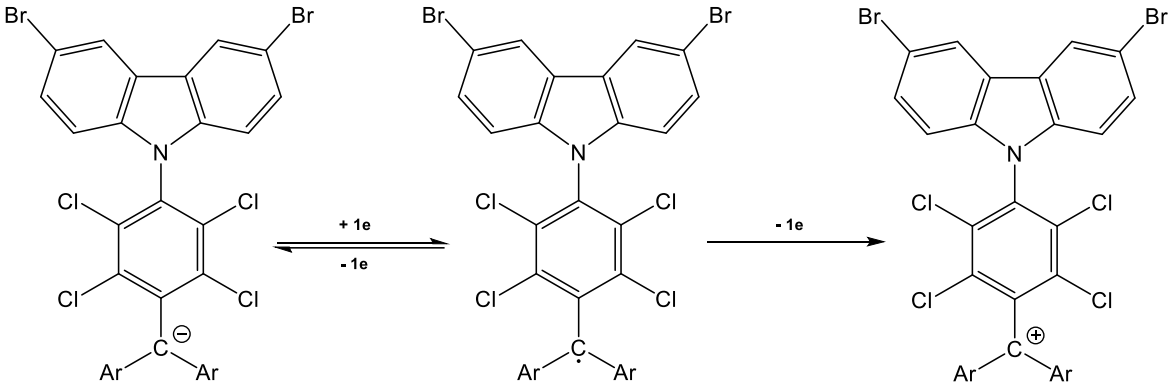

Fig. 44. Both redox processes represented with oxidized (right) and reduced (left) form of 2.*

Values of the electrochemical parameters are shown in Table 5. Reduction process is quasi-reversible because the difference between their anodic and cathodic peak potentials is always higher than the theoretical value of 59 mV expected for a one-electron reversible process. Its standard potential (E°) was determined as the average of the anodic ($E_{p,a}$) and cathodic ($E_{p,c}$) peak potentials. Electron affinity (EA), ionization potential (IP) and band gap (E_{gap}) were obtained with Eq. 8 and Eq. 9 from chapter 3.8.3.

E^{o}_{ox} (V) (($E_{p,a} - E_{p,c}$) (mV))	E^{o}_{red} (V) (($E_{p,a} - E_{p,c}$) (mV))	$E_{onsetOx}$ (V)	$E_{onsetRed}$ (V)	IP (eV)	EA (eV)	E_{gap} (eV)
-	-0.125 (70)	1.52	-0.06	6.12	4.54	1.58

Table 5. Electrochemical parameters values.

E_{onset} values were obtained graphically as it is shown by Fig. 45. In addition, IP and EA values are indeed the energy from HOMO and LUMO of **2*** respectively.

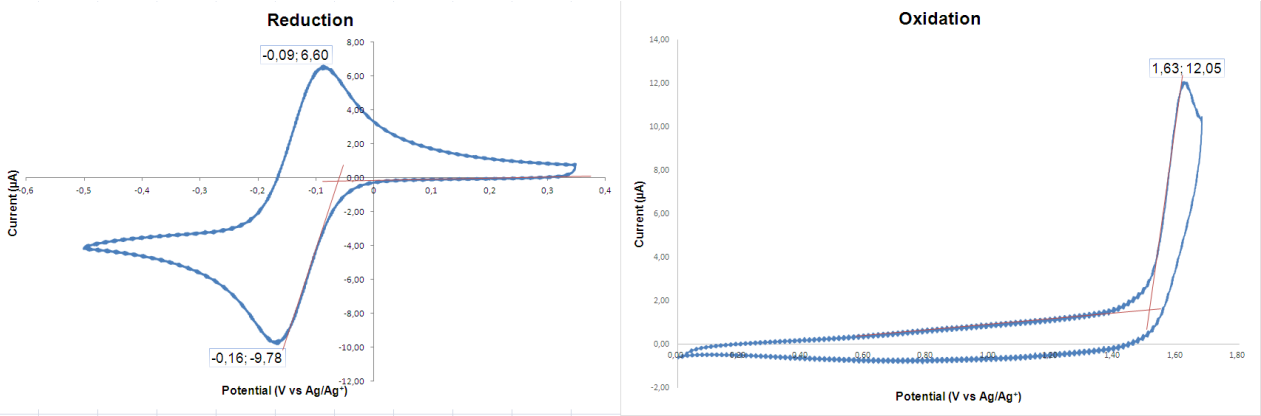

Fig. 45. Determination of potential onset value graphically in both processes.

Hence, it can be seen on Fig. 46 that as quicker scan rate goes, the peak difference ($E_{p,a}$ - $E_{p,c}$) increases.

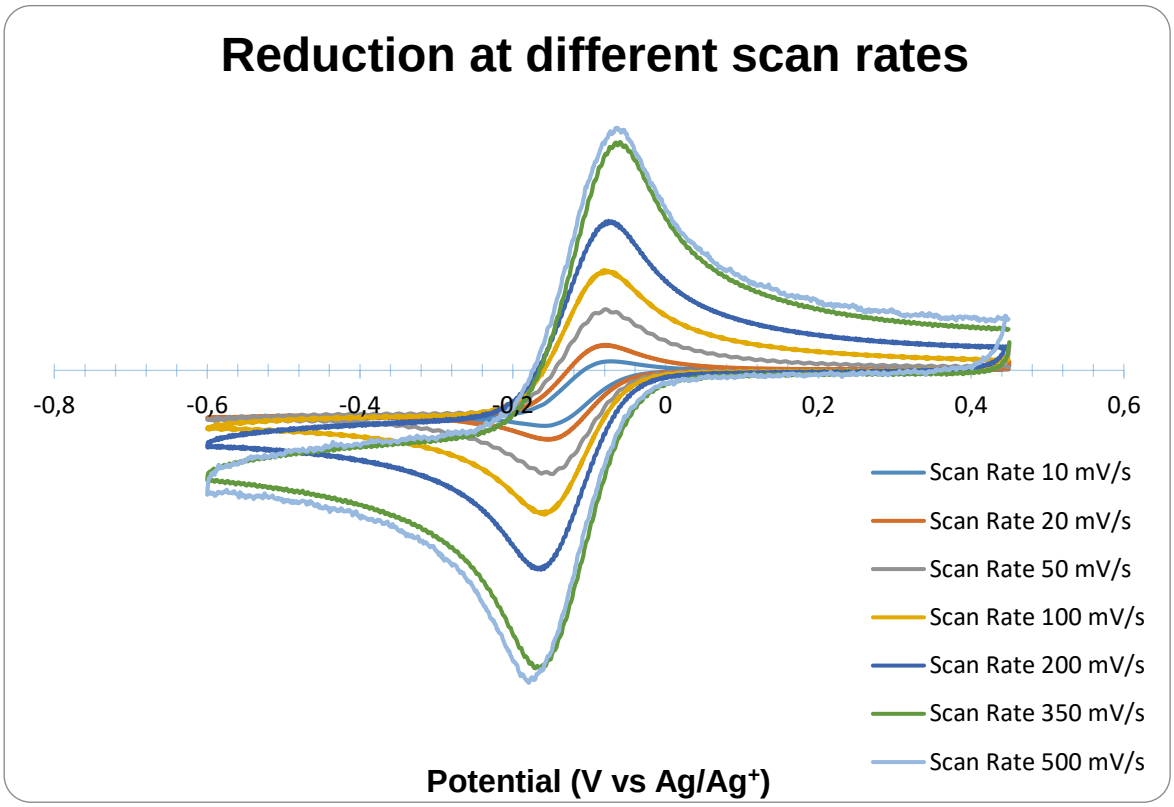

Fig. 46. Radical adduct reduction at different scan rates.

5.4. TGA and DSC characterization of radical adduct 2*

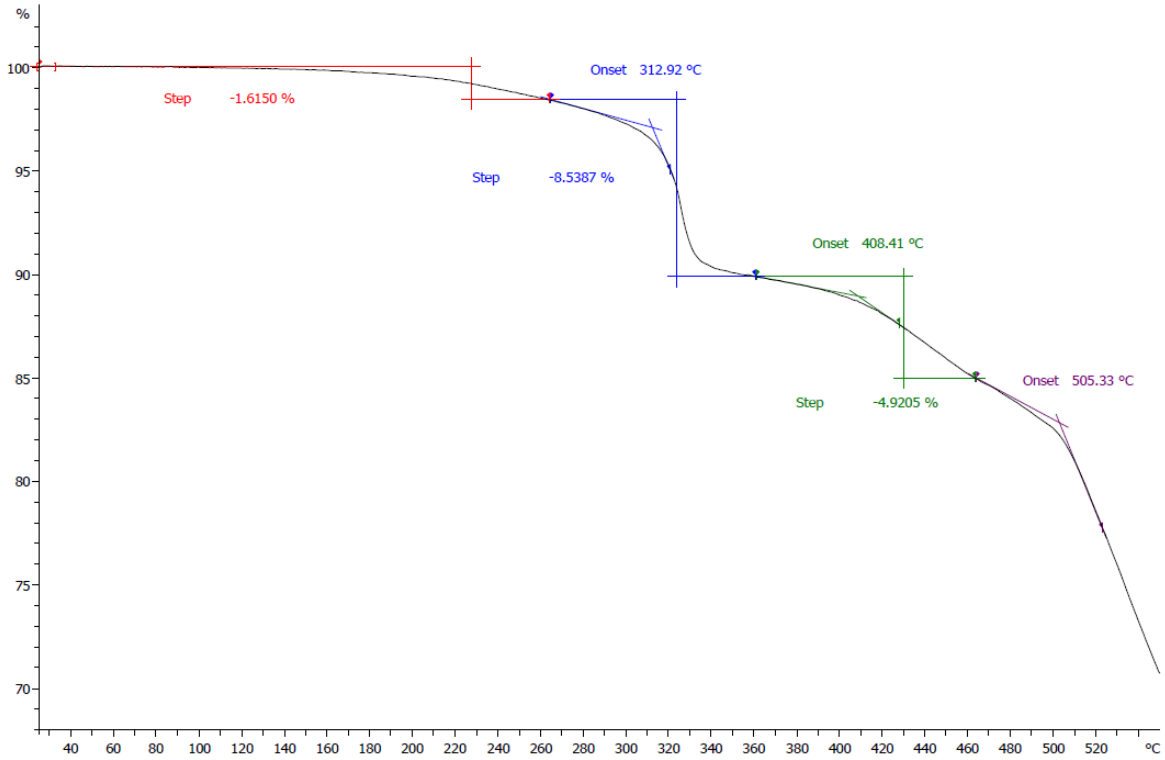

Fig. 47. TGA thermogram of 2. It can be seen two different degradation processes (blue and green).*

On one hand, Fig. 47 shows the result of thermogravimetric analysis (TGA) of radical adduct **2***. The first step of weight loss corresponds to solvent evaporation of the sample (1.62 %), which is marked in red colour. The second step of weight loss is the first decomposition reaction of **2*** (8.54 %), where the loss of two chloride atoms generate a molecular cyclization between benzenes. The decomposition temperature is indicated as *onset temperature* and, in this case, is 312.92 ºC. Furthermore, green slope change indicates the beginning of total decomposition of the product. It begins with 4.92 % weight loss in spite of a further unstoppable decomposition with temperature increase. This final degradation has an *onset temperature* of 408.41 ºC.

On the other hand, Fig. 48 shows differential scanning calorimetry (DSC) result, where endothermic and exothermic processes are illustrated. The product, when arrives at 308.75 ºC, experiments an exothermic process previously to its melting, as it starts absorbing heat at 321.84 ºC. Thus, when the sample arrives at 327.27 ºC, the first degradation reaction continues and the product unleashes a great amount of heat compared to the other processes.

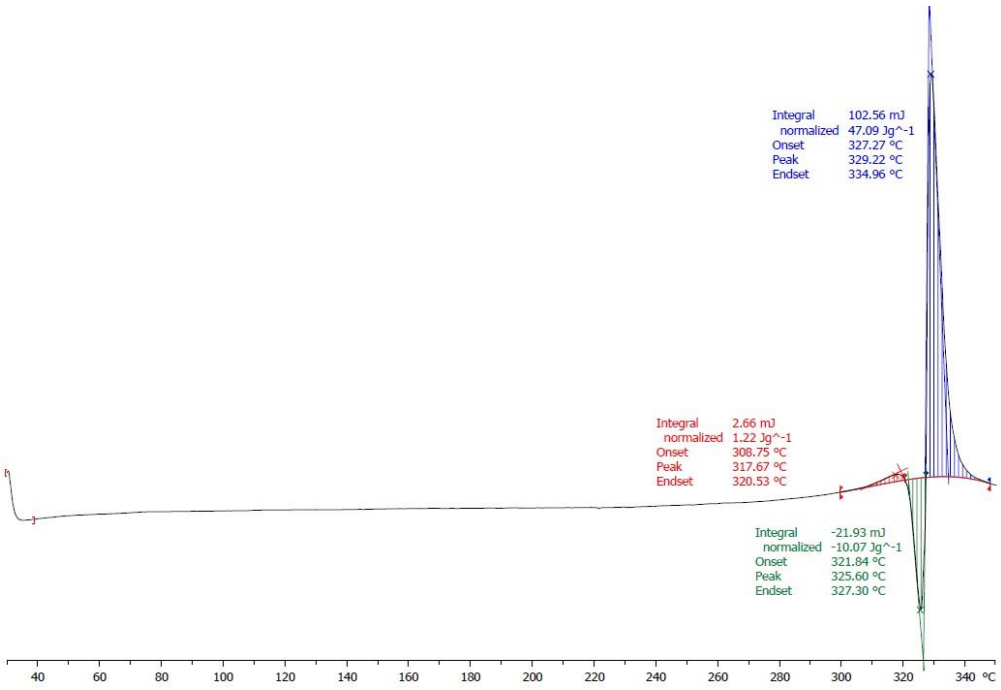

Fig. 48. DSC thermogram of 2.*

Finally, on Fig. 49, it can be seen a combination of graphics TGA and DSC. It is shown the relationship between these techniques and how the mass loss affects on energetic sample behaviour (absorption and release of heat).

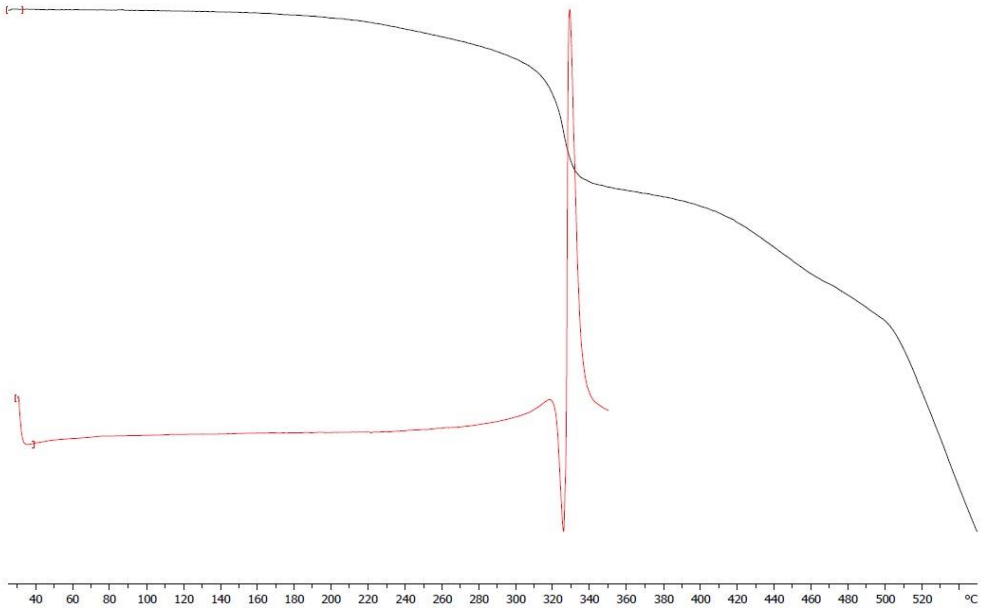

Fig. 49. TGA and DSC thermograms. DSC only shows heat transfer processes of the first degradation reaction.

6. Project schedule planning

This project has a length of 4 month, concretely 18 weeks to accomplish the experimental part and memory elaboration. In fact, the planning involves three main activities, the two mentioned above and a bibliographic search.

Traditionally, bibliographic search is done on the first couple of weeks before starting any other part of the project. Nevertheless, as the experimental part was predicted to be laborious, it was started as soon as possible. Furthermore, bibliographic search was kept along the schedule until the end because it was necessary to search information every time.

Experimental part is divided in two principal parts: synthesis and characterization. Synthesis has also been separated in two section as it was planned to synthesize two different radical adduct. For **1***, it was given 10 weeks because it was necessary to perform between five and seven reactions whereas for **2***, it was only required two. Characterization, as it was exposed on chapter 3.8, was composed of four techniques (UV-Vis, EPR, CV, TGA - DSC). It only took two weeks to complete them.

Finally, memory elaboration was planned for the last four weeks but, truly, it was started earlier when some results were obtained. However, the last four weeks were completely focused to elaborate it.

On Table 6 is showed a Gantt diagram of schedule planning explained above.

Week / Activity name	1	2	3	4	5	6	7	8	9	10	11	12	13	14	15	16	17	18
Bibliographic search	■	■	■	■	■	■	■	■	■	■	■	■	■	■	■	■	■	■
Experimental part - Synthesis of 1*	■	■	■	■	■	■	■	■	■	■								
Experimental part - Synthesis of 2*											■	■						
Experimental part - Characterization													■	■				
Memory elaboration															■	■	■	■

Table 6. Project's Gantt diagram.

7. Economical evaluation

The economical evaluation of this project is divided in four parts: reagents and material costs, equipment costs, energetic cost and employee expenses. Thus, it will be a final chapter where all the costs and expenses are summed up to obtain the final value of the developed project.

7.1. Reagents and material costs

In this chapter, a list of different reagents and material used through the project will be given (Table 7 and Table 8 respectively). Depending on the used quantity, a total cost will be calculated. The cost of each reagent and solvent was acquired from SigmaAldrich webpage.[36] Likewise, material costs were collected from FisherScientific webpage. [37]

Product	Quantity (L) Quantity (g)	Unitary Cost (€/L) Unitary Cost (€/g)	Total cost (€)
1,2-dichloroethane	0.12	132.00	15.84
Acetone	6	43.25	259.50
AcOH	0.05	49.00	2.45
Ar_2 gas	1	154.50	154.50
Ascorbic acid	2	0.65	1.30
C_6H_{12}	0.05	62.50	3.13
Carbazole	6	0.47	2.82
$CHCl_3$	5	48.80	244.00
Chloranil	3.5	5.00	17.50
Cs_2CO_3	3	3.18	9.54
DCM	0.02	47.00	0.94
Distilled water	5	0.80	4.00
DMF	0.06	83.50	5.01

Product	Quantity (L) Quantity (g)	Unitary Cost (€/L) Unitary Cost (€/g)	Total cost (€)
DMSO	0.01	770.00	7.70
EtOAc	0.30	55.00	16.50
EtOH	0.8	132.00	105.60
HCl	1.5	28.00	42.00
Hexane	5	86.50	432.50
HNO_3	0.02	359.00	7.18
KOH	25	0.13	3.25
Na_2SO_4	100	0.11	11.00
$NaHCO_3$	500	0.05	25.00
NaOH	100	0.10	10.00
Silica gel	6 200	0.12	744.00
$SnCl_2$	20	0.50	10.00
TBAOH	0.01	590.00	5.90
THF	0.5	15.0	77.00
Toluene	0.05	66.00	3.30
TOTAL:			**2 221.46 €**

Table 7. List of reagents and solvent used along the project. For each product, total cost was calculated by multiplying unitary cost by quantity.

The quantities on Table 7 were rounded up. Concretely, silica gel was estimated considering 400 ml/column and a density of 2,21 kg/L (seven chromatography columns were done).

Material	Units (u)	Unitary Cost (€/u)	Total cost (€)
Boiling flask 25 mL	1	9.46	9.46
Boiling flask 50 mL	1	19.03	19.03

Material	Units (u)	Unitary Cost (€/u)	Total cost (€)
Boiling flask 100 mL	1	15.64	15.64
Boiling flask 250 mL	1	28.11	28.11
Boiling flask 500 mL	1	35.74	35.74
Erlenmeyer 100 mL	6	28.97	173.82
Erlenmeyer 250 mL	7	30.37	212.59
Erlenmeyer 1 L	1	28.81	28.81
Beaker 50 mL	1	4.38	4.38
Beaker 100 mL	1	4.30	4.30
Beaker 250 mL	1	4.85	4.85
Beaker 600 mL	1	7.28	7.28
Volumetric flask 10 mL	2	5.90	11.80
Volumetric flask 25 mL	1	6.09	6.09
Chromatography column 0,7 L	1	79.15	79.15
Quartz cuvette 10 mm	1	52.00	52.00
Separation chamber (TLC)	1	108.73	108.73
TLC Plate – ALUGRAM aluminium sheets	4	8.61	34.43
Micropipettes 10 µL	1	0.10	0.10
Male with coupled olive	1	28.22	28.22
Angled tweezers	1	7.90	7.90
Normal tweezers	1	8.35	8.35
Retort stand	1	22,05	22,05
Utility clamp	2	43.13	86.26
Vacuum filter flask 500 mL	1	28.73	28.73
Filtration rubber joint	1	2.10	2.10

Material	Units (u)	Unitary Cost (€/u)	Total cost (€)
Glass funnel filter N°4 (Ø: 40mm)	1	43.56	43.56
Glass funnel filter N°4 (Ø: 65mm)	1	63.58	63.58
Plastic powder funnel (Ø: 80mm)	1	34.67	34.67
Plastic plain funnel (Ø: 80mm)	1	3.25	3.25
Plastic plain funnel (Ø: 65mm)	1	2.30	2.30
Plastic plain funnel (Ø: 45mm)	1	2.03	2.03
Decanting funnel 500 mL	1	48.59	48.59
Glass stopper	1	5.47	5.47
Dimroth condenser 250 mm	1	70.57	70.57
Rubber tube 1m	1	7.80	7.80
Spirit thermometer	1	2.27	2.27
Addition funnel 20 mL	1	74.55	74.55
Spoon/Spatula 150 mm	1	5.71	5.71
Spoon/Spatula 230 mm	1	3.50	3.50
Metal joint clamp	1	9.19	9.19
Steel clips	2	3.67	7.34
Magnetic stirrer bar 30 mm	1	3.86	3.86
Oval magnetic stirrer bar 20 mm	1	9.33	9.33
Glass Pasteur pipet	10	0.03	0.30
Glass vial 4 mL	10	0.43	4.30
$CaCl_2$ tube	1	8.29	8.29
Plastic balloon	2	0.20	0.40
Graduated cylinder 10 mL	1	11.13	11.13
Graduated cylinder 25 mL	1	9.95	9.95

Material	Units (u)	Unitary Cost (€/u)	Total cost (€)
Pipette tips 100-1000	5	0.02	0.10
Pipette tips 20-200	5	0.01	0.05
Weighing funnel	1	15.65	15.65
Rubber teat	5	0.92	4.60
Graduated cylinder 500 mL	1	44.03	44.03
TOTAL:			**1 494.24 €**

Table 8.List of material used along the project. For each element, total cost was calculated by multiplying unitary cost by quantity.

Thus, the reagent and material cost value ascend to 3 715.70 €.

7.2. Equipment costs

Equipment costs are divided in two blocks: expenses generated by uses of internal equipment and the cost of external analysis.

On one hand, the first type of cost was estimated for all different equipment used along the project. With Eq. 10, it is applied a constant amortization factor for each apparatus depending on acquisition cost, residual value and useful life. In all cases, the residual value is null as it is supposed that the equipment will last until its useful life is completed.

$$Equippment\ cost\ (€/month) = \frac{Acquisition\ cost\ (€) - Residual\ value\ (€)}{Useful\ life\ (years) \cdot 12}$$

(Eq. 10)

On Table 9 is shown a resume of this first type of cost. Prices are picked up from FisherScientific [37], 3Bscientific [38] and Labcomecial [39] webpages.

Equipment	Acquisition cost (€)	Useful life (years)	Activity period (months)	Total cost (€)
Analytical balance	1 200.00	20	4	20.00
Top loading balance	53.00	20	4	0.88
Heating magnetic stirrer	31..95	10	4	10.50
Rotary evaporator	2 742.00	20	4	45.70
Oven	975.67	20	4	16.26
UV-Vis Spectrophotometer	4 536.29	20	4	75.60
Micropipette 100-1000 µL	90.75	5	4	6.05
Micropipette 20-200 µL	90.75	5	4	6.05
TOTAL:				**181.04 €**

Table 9.List of equipment used along the project. For each element, total cost was calculated by using Eq. 10.

In the case of heating magnetic stirrer, the acquisition cost includes two hemispheric bowls (for 50 and 100 mL boiling flasks). The same happens with the rotary evaporator, which includes as accessories a receiving flask.

On the other hand, Table 10 resumes the cost of external analysis that is calculated with the real rates from IQAC-CSIC [34] and UB [40] services. Analysis such as IR, EPR, TGA, DSC and ^{1}H-NMR were done at IQAC-CSIC. Nevertheless, the other ones (CV, MS and ESI-HRMS) were carried out at UB facilities.

Service	Number of samples	Required time (min per sample)	Cost (€/h) Cost (€/sample)	Total cost (€)
EPR	1	60	10.00	10.00
ESI-HRMS	4	-	96.80	387.20
IR	25	10	10.00	41.67
^{1}H-NMR	3	5	12.00	3.00
CV	1	-	33.50	33.50
TGA	1	60	14.00	14.00
DSC	1	40	14.00	9.33
MS	1	-	5.50	5.50
TOTAL:				**504.20 €**

Table 10. List of external analysis with their corresponding price. Depending on number of samples, a total cost is calculated.

Finally, if both costs are summed up, the final cost for project equipment ascend to 685.25 €.

7.3. Energetic cost

Energetic cost of this project is divided in two fundamental parts:

- Water consumption due to material cleaning in addition to reaction and rotary evaporator refrigeration.
- Electricity consumption generated by different apparatus.

In case of water, Table 11 resumes diverse factors or specific points to take into account when water expenses are calculated. Certain duties like water supply fee, service fee or water meter and maintenance tasks are not computed, as they do not depend on this project fulfilment. This Table is based on a bill format from IQAC-CSIC centre, leading to use real taxes specifically for its geographic location [41].

	Volume (m^3)	Unitary cost (€/m^3)	Total cost (€)	IVA (%)
Water consumption	7.93	1.29	10.23	10
General tax rate	7.93	0.1654	1.31	
Specific tax rate	7.93	0.6486	5.14	
Water canon	7.93		6.45	10
IVA 10 %			1.67	
Until 12 m^3	7.93	0.1529	1.21	
More than 12 m^3	0	0.2294	0.00	
Sewerage tax rate			1.21	
Metropolitan Tax for Municipal waste Treatment (M.T.M.T.)			21.67	
TOTAL			**41.23 €**	

Table 11. Water expenses breakdown.

Furthermore, water flow measures resulted on a refrigeration flow of 0.042 m^3/h and a cleaning flow of 0.166 m^3/h.

Assuming a 15 min/day use of cleaning flow during 57 days (project's experimental time) and a refrigeration flow utilization during 106.5 h (total reaction time) and 26 days (half of synthesis days, one hour per day) using rotary evaporator, concludes on 7.93 m^3 of water consumption.

In the case of electricity, it is only considered the cost of electricity consumption (€/kWh), electrical taxes [42] and IVA (21 %). Fix cost associated to hired potency and electric meters are not taking in account as they do not depend on this project fulfilment. From 2018 CSIC-IQAC electricity bills, it is known that hired potency is 800 kW (high voltage) and a cost of 0.06698 €/kWh is estimated. The last cost was calculated considering tariff type (ATR: 6.1A) and between which hour range electricity was consumed (8 to 14 h). Table 12 resumes electricity expenses.

	Potency (W)	Utilization time (h)	Total cost (€)
Analytical balance	20	6	0.00804
Top loading balance	60	0.5	0.00201
Oven	2400	60	9.64512
Rotary evaporator	100	40	0.26792
Heating magnetic stirrer	750	106.5	5.35003
UV-Vis Spectrophotometer	180	25	0.30141
Electricity consumption (EC)			15.57
Electrical taxes (5.11269632 % x EC)			0.80
IVA (21 %)			3.44
TOTAL			**19.81 €**

Table 12. Electricity expenses breakdown.

7.4. Employee expenses

For employee expenses, it has been considered a junior chemical engineer and a scientific investigator that acts as project guider and supervisor.

The XVIII general agreement of chemical industry [43], as well as Art. 32 CE 2017 [44], specifies a minimum gross salary of 25 614.73 €/year for junior chemical engineer (professional category 6). For the scientific investigator, a gross salary around of 71 500 €/year is expected.

To calculate the real expenses, it is necessary to add 32 % of gross salary as Social Security (SS) payment in charge of the firm and to consider 1760 h/year as working hours' average. [45] Table 13 show a resume of these expenses.

Employee	Gross salary (€/year)	Salary per hour (€/h)	Worked hours (h)	Full salary (€)	SS expenses (€)	Total cost (€)
Junior chemical engineer	25 614.73	14.55	600	8 730	2 793.60	11 523.60
Scientific investigator	71 500	40.63	120	4 875	1 560	6 435
TOTAL:						**17 958.60€**

Table 13. Junior chemical engineer and scientific investigator expenses.

7.5. Total cost

Project's total cost is formed by addition of the results obtained from the last four subchapters. This is represented on Table 14.

Type of cost	Cost (€)	Percentage (%)
Reagents and material costs	3 715.7	16.57
Equipment costs	685.24	3.06
Energetic cost	61.04	0.27
Employee expenses	17 958.60	80.10
TOTAL	**22 420.58 €**	

Table 14. Costs and expenses summary.

To conclude this chapter, it can be seen that higher costs generated by this project are employee expenses with an 80.10 % of global cost. In contrast, equipment and energetic costs represent a minority part of the whole amount.

8. Environmental impact assessment

When an investigation project is done, it carries behind itself an environmental impact that is important to minimize. Thus, it is of great relevance to discharge wastes into specific containers, minimize vapours releases to the atmosphere with the use of extractor hood, waste less water as possible and not exceed electrical consumption.

8.1. Residue management

Any residue generated along the project has to be classified in accordance to its physicochemical properties, dangerousness and further treatment. In addition, it is necessary to plan a selective collection of them besides labelling correctly the containers.

On Table 15 there is a list of different residue categories stablished by IQAC-CSIC centre. [46]

Classification	Description	Example
Halogenated solvents	Any liquid organic product with more than 2 % of halogen.	DCM or $CHCl_3$
Non-halogenated solvents	Any liquid organic product with less than 2 % of halogen.	EtOH or DMF
Aqueous solutions	This group is divided in organic/inorganic products with/without halogen, heavy metals, etc.	NaOH, Phosphates, etc.
Acids	Formed by inorganic acids or its solution with more than 10 % (Vol.) concentration.	H_2SO_4, HNO_3 (concentrated)
Oils	Mineral oils generated by maintenance operations	-
Solid products	Solid chemical products organic/inorganic	Silica gel or active carbon
Especial products	Products of high toxicity or dangerousness	Peroxide or fuming acids

Contaminated glass	-	Empty glass bottles
Contaminated plastic	-	Empty plastic bottles
Contaminated metal	-	Metal package
Cytostatic	Carcinogenic, mutagen or teratogenic products	Contaminated material with phenol
Biodangerous products	Sanitary residues	Petri dishes

Table 15. Classification depending on residue nature.

Furthermore, there is a list of solvent safety data sheet on chapter B (see annex).

8.2. Water consumption

Despite producing residues, it is also essential to consider water consumption. As it was calculated on chapter 7.3, 7.93 m^3 from water supply network is consumed along the project.

8.3. CO_2 generation

The last point to consider in this chapter is how many equivalent kg of CO_2 are generated with this project development. With the help of the *Oficina Catalana del Canvi Climàtic* (OCCC), it can be calculated this value depending on energetic consumption. [47] This involves water and electricity, and for this year, OCCC has given an emission rate associated to electric energy of 392 g CO_2/kWh, and for water waste of 395 g CO_2/m^3 H_2O. Table 16 resumes the total amount of equivalent CO_2 generated.

Type of source	Consumption (m^3) Consumption (kWh)	Emission rate (Kg CO_2/m^3) Emission rate (Kg CO_2/kWh)	CO_2 (Kg)
Water	7.93	0.395	3.13
Electricity	232.53	0.392	91.15
TOTAL			**94.28 Kg CO_2**

Table 16. CO_2 generation breakdown.

Conclusions

In this chapter, it will be brought out conclusions from the initial objectives marked at the beginning of this project contrasted with the results collected:

- Radical adduct **2*** has been successfully synthesized (reaction yield of 33 %). IR, ESI-HRMS and MS confirmed its identify and purity. Despite radical adduct **1*** was tried to synthesize by three different synthetic paths, none of them resulted successfully.

- UV-Vis absorption spectroscopy has shown that **2*** has charge-transfer properties because at 629 nm (DCM solvent) appears an specific and additional band that the components of this radical adduct, 3,6-BrCz or DTM, lack it. Comparing this charge-transfer band with that of previous radical adducts, synthesized by NFR research group, it is concluded that **2*** has better charge transfer properties than CzDTM but worse than CH_3OCzDTM. The explanation to this is that at higher wavelength, the charge-transfer band is less energetic, leading to a more stable excited state.

- EPR analysis has corroborated the radical character of **2***. Thus, considering parameters extracted at 298 K and 223 K, spin density is mainly situated on trivalent carbon. In addition, carbazole moiety do not influence on radical character of **2***, as its nitrogen atom do not appear in any spectra.

- CV results have shown a quasi-reversible reduction process and an irreversible oxidation process for radical adduct **2***. The E_{gap} obtained was good enough to use this radical as organic semiconductor.

- TGA – DSC analysis showed that radical adduct **2*** is stable until 313 ºC, when the radical adduct starts a degradation reaction corresponding with its melting. Nevertheless, total decomposition starts when a temperature of approximately 408 ºC is reached.

- A large economical evaluation of this project have been done analysing reagents and material, equipment and energetic costs with the addition of employee expenses. Results determined that employee expenses represented the majority of costs with approximately 80 % of the whole amount.

- An environment impact assessment have been done to analyse in which ways this project has affected to the environment. It has been mentioned how to classify the residues depending on their dangerousness and origin, how much water has waste and how many kilograms of CO_2 have been produced.

Acknowledgments

I want to express my full gratitude to Dr. Lluís Julià for welcoming me in his investigation group at CSIC-IQAC centre and for explaining everything I know now about radical adducts, chemistry synthesis and characterization techniques. Without his gentleness and dedication, it would not have been possible to realise this project with success.

In addition, I want to thank Dr. Maria Pilar Almajano for bringing this opportunity to me as I expressed to her my restlessness for learning more about chemistry.

Furthermore, I want to thank Dr. Maria Dolors Velasco and Dr. Jaume Garcia Amorós from UB for the possibility to use cyclic voltammetry equipment and for the explanation of this technique.

Moreover, I really want to thank to all the RUBAM crew for welcoming me and make my stance at CSIC-IQAC centre more enjoyable from the first day, especially to Sofía for advise me how to write the chemical part of this project and helping me with it.

Finally, to my parents to support me unconditionally every day.

Thanks to all involved with me in these months, because without you it would not have been the same.

References

Bibliographical references

[1] University of Michigan, “THE DISCOVERY OF ORGANIC FREE RADICALS BY MOSES GOMBERG.” American Chemical Society, 2000.

[2] M. Gomberg, “AN INSTANCE OF TRIVALENT CARBON: TRIPHENYLMETHYL.,” *J. Am. Chem. Soc.*, vol. 22, no. 11, pp. 757–771, Nov. 1900.

[3] M. Ballester, J. Riera, J. Castafier, C. Badía, and J. M. Monsó, “Inert carbon free radicals. I. Perchlorodiphenylmethyl and perchlorotriphenylmethyl radical series,” *J. Am. Chem. Soc.*, 1971.

[4] S. Castellanos, D. Velasco, F. López-Calahorra, E. Brillas, and L. Julia, “Taking advantage of the radical character of tris(2,4,6-trichlorophenyl) methyl to synthesize new paramagnetic glassy molecular materials,” *J. Org. Chem.*, 2008.

[5] Z. Shufen, Z. Danhong, and Y. Jinzong, “Nitration of Carbazole and N-Alkylcarbazoles,” *Dye. Pigment.*, vol. 27, no. 4, pp. 287–296, 1995.

[6] A. Dangsopon, N. Poomsuk, K. Siriwong, T. Vilaivan, and C. Suparpprom, “Synthesis and fluorescence properties of 3,6-diaminocarbazole-modified pyrrolidinyl peptide nucleic acid,” *RSC Adv.*, 2016.

[7] M. Ballester, J. Riera, J. Castañer, and M. Casulleras, “The reduction of inert free radicals with ascorbic acid. The reaction with perchlorotriphenylmethyl radical,” *Tetrahedron Lett.*, vol. 19, no. 7, pp. 643–644, Jan. 1978.

[8] D. Velasco, S. Castellanos, M. López, F. López-Calahorra, E. Brillas, and L. Juliá, “Red Organic Light-Emitting Radical Adducts of Carbazole and Tris(2,4,6-trichlorotriphenyl)methyl Radical That Exhibit High Thermal Stability and Electrochemical Amphotericity,” *J. Org. Chem.*, vol. 72, no. 20, pp. 7523–7532, Sep. 2007.

[9] V. Gamero, D. Velasco, S. Latorre, F. López-Calahorra, E. Brillas, and L. Juliá, “[4-(N-Carbazolyl)-2,6-dichlorophenyl]bis(2,4,6-trichlorophenyl)methyl radical an efficient red light-emitting paramagnetic molecule,” *Tetrahedron Lett.*, 2006.

[10] L. Fajarí *et al.*, “Charge transfer states in stable neutral and oxidized radical adducts from carbazole derivatives,” *J. Org. Chem.*, 2014.

[11] S. A. Holgate, *Understanding Solid State Physics.* CRC Press, 2009.

[12] C. Kittel, *Introduction to solid state physics*, Seventh. New York: Wiley, 1996.

[13] E. Lupon and UPC, “T3 - Introducció als semiconductors.” Barcelona, 2017.

[14] Y. Shirota, M. Kinoshita, T. Noda, K. Okumoto, and T. Ohara, “A Novel Class of Emitting

Amorphous Molecular Materials as Bipolar Radical Formants: 2-{4-[Bis(4-methylphenyl)amino]phenyl}- 5-(dimesitylboryl)thiophene and 2-{4-[Bis(9,9-dimethylfluorenyl)amino]phenyl}- 5-(dimesitylboryl)thiophene," *J. Am. Chem. Soc.*, vol. 122, no. 44, pp. 11021–11022, Nov. 2000.

[15] B. K. Crone, I. H. Campbell, P. S. Davids, D. L. Smith, C. J. Neef, and J. P. Ferraris, "Device physics of single layer organic light-emitting diodes," *J. Appl. Phys.*, vol. 86, no. 10, pp. 5767–5774, 1999.

[16] S. Gelinas *et al.*, "Ultrafast Long-Range Charge Separation in Organic Semiconductor Photovoltaic Diodes," *Science (80-.).*, vol. 343, no. 6170, pp. 512–516, Jan. 2014.

[17] J. Nelson, "Organic photovoltaic films," *Curr. Opin. Solid State Mater. Sci.*, vol. 6, no. 1, pp. 87–95, 2002.

[18] H. Hoppe and N. S. Sariciftci, "Organic solar cells: An overview," *J. Mater. Res.*, vol. 19, no. 07, pp. 1924–1945, Jul. 2004.

[19] C. Reese, M. Roberts, M. Ling, and Z. Bao, "Organic thin film transistors," *Mater. Today*, vol. 7, no. 9, pp. 20–27, Sep. 2004.

[20] H. Klauk, "Organic thin-film transistors," *Chem. Soc. Rev.*, vol. 39, no. 7, pp. 2643–2666, 2010.

[21] A. A. Edwards and B. D. Alexander, "Organic Applications of UV-Visible Absorption Spectroscopy," in *Encyclopedia of Spectroscopy and Spectrometry*, Elsevier, 2010, pp. 2030–2039.

[22] D. A. Skoog and Donald M. West, *Principles of instrumental analysis*, Second Edi. Philadelphia: Saunders College, 1980.

[23] RSC, "Ultraviolet -Visible Spectroscopy (UV)," *R. Soc. Chem.*, p. 7, 2009.

[24] G. W. Brudvig, "Electron paramagnetic resonance spectroscopy," 1995, pp. 536–554.

[25] C. C. Rowlands and D. M. Murphy, "EPR Spectroscopy, Theory Basic Principles of the EPR Experiment," *Encycl. Spectrosc. Spectrom.*, pp. 517–526, 2017.

[26] M. J.N.Junk, *Assessing the Functional Structure of Molecular Transporters by EPR Spectroscopy*. 2012.

[27] The resonance, "EPR Spectrometer | ESR Spectroscopy." [Online]. Available: https://www.theresonance.com/epr-101/. [Accessed: 17-Mar-2018].

[28] A. R. Barron and C. Bovet, "Basic principles for EPR spectroscopy," pp. 1–4, 2009.

[29] N. Elgrishi, K. J. Rountree, B. D. McCarthy, E. S. Rountree, T. T. Eisenhart, and J. L. Dempsey, "A Practical Beginner's Guide to Cyclic Voltammetry," *J. Chem. Educ.*, vol. 95, no. 2, pp. 197–206, 2018.

[30] G. A. Mabbott, "An introduction to cyclic voltammetry," *J. Chem. Educ.*, vol. 60, no. 9, p. 697, Sep. 1983.

[31] “Differential Scanning Calorimetry and Thermogravimetric Analysis,” in *Solid State Properties of Pharmaceutical Materials*, Hoboken: John Wiley & Sons, Inc., 2017, pp. 124–141.

[32] EAG Laboratories, “Characterization of Polymers using Differential Scanning Calorimetry (DSC).” [Online]. Available: https://www.eag.com/resources/whitepapers/characterization-of-polymers-using-differential-scanning-calorimetry-dsc/. [Accessed: 04-May-2018].

[33] A. W. Coats and J. P. Redfern, “Thermogravimetric analysis. A review,” *Analyst*, vol. 88, no. 1053, p. 906, 1963.

[34] IQAC-CSIC, “Magnetic Resonance Services.” [Online]. Available: http://www.iqac.csic.es/index.php?option=com_ogngrups&view=service_facility&Itemid=96&cid=55&lang=en. [Accessed: 17-May-2018].

[35] H. Zhang, X. Wan, X. Xue, Y. Li, A. Yu, and Y. Chen, “Selective Tuning of the HOMO-LUMO Gap of Carbazole-Based Donor-Acceptor-Donor Compounds toward Different Emission Colors,” *European J. Org. Chem.*, vol. 2010, no. 9, pp. 1681–1687, Mar. 2010.

[36] “Spain | Sigma-Aldrich.” [Online]. Available: https://www.sigmaaldrich.com/spain.html. [Accessed: 26-May-2018].

[37] “Fisher Scientific Spain: Laboratory Equipment and Supplies.” [Online]. Available: https://www.fishersci.es/es/en/home.html. [Accessed: 17-May-2018].

[38] “Simuladores médicos, modelos anatómicos y tablas, terapia, equipamiento para acupuntura y masajes, suministros para física y biología - 3B Scientific.” [Online]. Available: https://www.3bscientific.es/. [Accessed: 17-May-2018].

[39] “Tienda online de material de laboratorio - LAB Comercial - Material de laboratorio.” [Online]. Available: https://www.labcomercial.com/es/. [Accessed: 17-May-2018].

[40] Universitat de Barcelona, “Tarifes dels serveis de l’Universitat de Barcelona al 2018.” UB, 2018.

[41] AGBAR, “Preus i tarifes - Aigües de Barcelona.” [Online]. Available: http://www.aiguesdebarcelona.cat/facturadelaigua/preus-tarifes/. [Accessed: 20-May-2018].

[42] D. De and J. Estado, “LEGISLACIÓN CONSOLIDADA Ley 37/1992, de 28 de diciembre, del Impuesto sobre el Valor Añadido.,” pp. 1–145, 1992.

[43] M. D. E. Educación and C. Y. Deporte, “Boletín oficial del estado,” *BOLETÍN Of. DEL ESTADO Miércoles 19 agosto 2015, núm. 198, Sec. III, pp. 75276 a 75399*, p. 75276 a 75399, 2015.

[44] A. y M. A. Ministerio de Agricultura, “Boletín Oficial Del Estado,” *BOLETÍN Of. DEL ESTADO Miércoles 15 febrero 2017, núm. 39, Sec. III, pp. 10327 a 10329*, pp. 10327–10329, 2017.

[45] M. de Educación, Cultura y Deporte, “Boletín oficial del estado,” *BOLETÍN Of. DEL ESTADO Jueves 25 enero 2018, núm. 22, Sec. III, pp. 9627 a 9644*, no. 25, pp. 9627–9644, 2018.

[46] R. Alonso, “Gestión de residuos CID-CSIC,” no. Cid. CID-CSIC.

[47] Generalitat de Catalunya, “Oficina Catalana del Canvi Climàtic (OCCC).” [Online]. Available: http://canviclimatic.gencat.cat/es/. [Accessed: 23-May-2018].

Other references

E. Bellmann, S. Shaheen, S. Thayumanavan, S. Barlow, R. Grubbs, S. Marder, B. Kippelen and N. Peyghambarian, "New Triarylamine-Containing Polymers as Hole Transport Materials in Organic Light-Emitting Diodes: Effect of Polymer Structure and Cross-Linking on Device Characteristics", *Chemistry of Materials*, vol. 10, no. 6, pp. 1668-1676, 1998.

A. Dangsopon, N. Poomsuk, K. Siriwong, T. Vilaivan and C. Suparpprom, "Synthesis and fluorescence properties of 3,6-diaminocarbazole-modified pyrrolidinyl peptide nucleic acid", *RSC Advances*, vol. 6, no. 78, pp. 74314-74322, 2016.

M. Grätzel, "Dye-sensitized solar cells", *Journal of Photochemistry and Photobiology C: Photochemistry Reviews*, vol. 4, no. 2, pp. 145-153, 2003.

H. Shirakawa, E. Louis, A. MacDiarmid, C. Chiang and A. Heeger, "Synthesis of electrically conducting organic polymers: halogen derivatives of polyacetylene", *Journal of the Chemical Society*, Chemical Communications, no. 16, p. 578, 1977.

M. Jørgensen, K. Norrman and F. Krebs, "Stability/degradation of polymer solar cells", *Solar Energy Materials and Solar Cells*, vol. 92, no. 7, pp. 686-714, 2008.

[8]A. Mikami, T. Koshiyama and T. Tsubokawa, "High-Efficiency Color and White Organic Light-Emitting Devices Prepared on Flexible Plastic Substrates", *Japanese Journal of Applied Physics*, vol. 44, no. 1, pp. 608-612, 2005.

C. Tang, "Two-layer organic photovoltaic cell", *Applied Physics Letters*, vol. 48, no. 2, pp. 183-185, 1986.